

Ensembles of center vortices and chains: Insights from a natural lattice framework

David R. Junior¹ and Luis E. Oxman²

¹*Instituto de Física Teórica, Universidade Estadual Paulista and
South-American Institute of Fundamental Research ICTP-SAIFR,*

Rua Dr. Bento Teobaldo Ferraz, 271 - Bloco II, 01140-070 São Paulo, SP, Brazil

²*Instituto de Física, Universidade Federal Fluminense, 24210-346 Niterói, RJ, Brasil.*

(Dated: November 8, 2024)

A scenario to understand the asymptotic properties of confinement between quark probes, based on a mixed ensemble of percolating center vortices and chains, was initially proposed by one of us in a non-Abelian setting. More recently, the same physics was reobtained by means of a Schrödinger wavefunctional peaked at Abelian-projected configurations, which deals with center-vortex lines and pointlike monopoles in real space. In this work, we will reassess both settings in the unified language provided by the Weingarten lattice representation for the sum over surfaces. In particular, in the phase where surfaces are stabilized by contact interactions and percolate, lattice gauge fields emerge. This generalizes the Goldstone modes in an Abelian loop condensate to the case where non-Abelian degrees of freedom are present. In this language, the different natural matching properties of elementary center-vortex worldsheets and monopole worldlines can be easily characterized. In the lattice, both the Abelian and non-Abelian settings implement the original idea that the mixed ensemble conciliates N -ality with the formation of a confining flux tube. Common features, differences in the continuum, and perspectives will also be addressed.

I. INTRODUCTION

Lattice studies have identified and analyzed the relevance of different topological degrees of freedom with the aim of understanding the confining properties of 4D Yang-Mills (YM) theories. Ensembles of percolating center-vortex worldsheets, which naturally accommodate the N -ality property observed at asymptotic distances [1], have been shown to play a central role [2–15]. More recently, the importance of center vortices in describing infrared physics even in the presence of dynamical fermions was shown in Refs. [16, 17]. In Ref. [18], it was proposed that mixed ensembles of center vortices and chains could integrate the various asymptotic properties of confinement in $SU(N)$ YM theory. This proposal was motivated by the N -ality properties of the former and the possibility to trigger a flux tube with the monopole component in chains, where elementary center vortices (center-charge ± 1) carrying different defining magnetic weights β_i , $i = 1, \dots, N$, are attached in pairs to monopoles with charge $\beta_i - \beta_j$. These collimated fluxes, also known as nonoriented center vortices, were observed in Abelian projected link-variables in Monte Carlo simulations of $SU(2)$ YM theory [19] and contribute to the topological charge [20]. In $SU(2)$, when these variables were further processed to get center projected ones, it was established that 61% of the configurations contained no monopoles, while the rest contained at least a monopole-antimonopole pair. For general N , it is interesting to note that this type of nonoriented configuration was recently shown to be a preferred saddle-point for YM in compactified spacetimes [21]. In Ref. [18], the modeling of the mixed ensemble was motivated by the lattice description of an Abelian ensemble of worldsheets coupled to an external Kalb-Ramond field [22]. In this context, the Goldstone modes for the loop condensate are represented by an Abelian gauge field. Then, in the center-vortex framework, we initially considered a Kalb-Ramond field to express the intersection number between a center-vortex worldsheet s and a surface whose border is the Wilson loop \mathcal{C}_e . This corresponds to the linking number between s and \mathcal{C}_e . When center vortices condense, this allowed for a representation of Wilson loop averages based on gauge-field Goldstone modes with

frustration. From that point on, instead of continuing with the Abelian description, chains and the natural correlations among center vortices were introduced through a non-Abelian extension to $SU(N)$. For example, N -matching properties, which is one of the hallmarks of center vortices, were naturally implemented (see [23] and Sec. II 2). In this way, the monopole component in collimated center-vortex chains as well as its condensation were shown to be essential for the formation of a confining flux tube between quarks. For a discussion of the properties captured from this ensemble perspective, see Refs. [24–26]. More recently, this type of four-dimensional mixed ensemble was studied in the Abelian-projected setting, at the level of the Hamiltonian formalism and the vacuum wavefunctional [27]. As this formalism deals with gauge fields defined on the real space \mathbb{R}^3 , we were able to apply techniques developed in Refs. [28, 29] for the 3D partition function in Euclidean spacetime. For percolating center-vortex only ensembles, the vacuum wavefunctional can be represented by a scalar field theory with a continuum vacua manifold. The Abelian-projected gauge fields for center-charge ± 1 vortices are, once more, naturally characterized by the N different yet physically equivalent defining magnetic weights β_i . Likewise, monopoles carrying charges $\beta_i - \beta_j$ on chains remained essential to trigger a Wilson loop area law. This component can turn the set of vacua discrete, thus leading to a domain wall sitting on the Wilson loop. Recently, center vortices only characterized by their center charge $1, \dots, N - 1$ were addressed in Ref. [30]. Interestingly, the proliferation of monopoles sitting at the junction of N charge 1 center vortices in theories with Z_N 1-form symmetry were shown to be crucial for confinement.

The main objective of this work is to compare the non-Abelian and Abelian-projected mixed ensembles by expressing them in a unified language—specifically, the Weingarten matrix representation of surfaces [31]. In Sec. II, we summarize the key physical inputs and previous developments regarding the modeling of mixed ensembles in four dimensions. In Sec. III, we briefly review the noninteracting $N \times N$ matrix models and interpret them as generating surfaces with N possible colors at the vertices. These models are stabilized by means of contact interactions in Sec. IV, which also helps to clarify the emergence of gauge-field Goldstone modes when surfaces percolate. In Sec. V, lattice ensembles of loops and lines are briefly reviewed. The 4D lattice description and implications of the Abelian-projected ensemble, formed by N surface types with global magnetic charges, is given in Sec. VI. In Sec. VII, this is compared with the non-Abelian setting, where the magnetic charges are locally distributed at surface vertices. Finally, Sec. VIII is devoted to the conclusions.

II. MIXED ENSEMBLES IN FOUR DIMENSIONS

Here, we shall briefly summarize the main physical inputs about mixed ensembles of center vortices and chains. Some of them have already been detected in the lattice, while others constitute natural possibilities. In this direction, the different lattice configurations have their counterpart in the continuum. The associated gauge fields A_μ can be parametrized by different singular mappings $S \in SU(N)$ together with appropriate profiles, so as to get thick collimated objects. These mappings encode the vortex guiding centers and the possible charges they carry (see Ref. [23] and references therein). Outside the center-vortex cores, where the field strength is zero, they also describe the local (but not global) pure gauge field A_μ .

1. Percolating center vortices

The confining phase is formed by large clusters of percolating center vortices [6, 17]. In Refs. [8, 11], a lattice random surface model that captures the order of the phase transition in $SU(2)$ and $SU(3)$ was proposed. This model is based on an action for oriented center-vortex worldsheets s

with stiffness, a property also observed in lattice simulations [32, 33]. At the level of the partition function, as well as in the wavefunctional formalism, we have been modeling ensembles formed by elementary center vortices (center charge ± 1). In the continuum, these configurations can be described by means of the mapping

$$S = e^{i\chi\beta\cdot T} \quad , \quad \beta\cdot T \equiv \beta|_q T_q \quad , \quad (1)$$

where χ is multivalued and changes by $\pm 2\pi$ when going around the vortex guiding-centers, T_q are the diagonal (Cartan) generators of $\mathfrak{su}(N)$, and β is one of the N magnetic weights $\beta_i = 2N\omega_i$ of the defining representation of $SU(N)$. The weights ω_i , $i = 1, \dots, N$, are formed by the elements of T_q at the i -th position of the diagonal.¹ Outside the center-vortex core, Eq. (1) corresponds to the gauge field

$$a_\mu = \partial_\mu \chi \beta \cdot T \quad . \quad (2)$$

When a Wilson loop in the defining representation is completely linked by the center-vortex flux once, the different vortex types β_i give the same elementary center-element $e^{\pm i2\pi/N}$, with a sign that depends on the loop orientation.

2. Center-vortex N -matching

As the defining magnetic weights satisfy

$$\beta_1 + \dots + \beta_N = 0 \quad ,$$

at a fixed time, configurations formed by N lines $\gamma_1, \dots, \gamma_N$ carrying weights β_1, \dots, β_N can be matched at a common endpoint [23, 27, 29]. In the continuum, an array with two common endpoints can be described in terms of the singular transformation

$$S = e^{i\chi_1\beta_1\cdot T} \dots e^{i\chi_{N-1}\beta_{N-1}\cdot T} \quad , \quad (3)$$

where χ_i is an angle that is multivalued with respect to the loop formed by $\gamma_i \circ (-\gamma_N)$. For $SU(3)$, this type of matching was observed in the lattice [34, 35].

3. Center vortices attached to monopoles (collimated chains)

Another important class of configurations is formed by collimated center-vortex fluxes attached in pairs to monopoles. These objects, known as chains or nonoriented center vortices (in the Lie algebra) were detected in $SU(2)$, with a procedure based on the Maximal Abelian gauge (MAG) [19]. Because of the monopoles, chains are essentially non-Abelian configurations [36]. For example, the guiding centers for a chain localized on the z -axis with a monopole at $z = 0$ is described by

$$S = e^{i\varphi\beta\cdot T} W(\theta) \quad , \quad W(\theta) = e^{i\theta\sqrt{N}T_\alpha} \quad , \quad (4)$$

where T_α is an off-diagonal generator. This phase characterizes the transition from a center-vortex weight β' to β , as we go from negative to positive z . This is mediated by a monopole with charge $\beta - \beta'$. As discussed in Ref. [27], the associated non-Abelian gauge field can be written as a singular gauge transformation of a Cartan gauge field. This is performed with a non-Abelian phase S_D ,

¹ The ‘‘magnetic’’ weights of a representation $D(\cdot)$ of $\mathfrak{su}(N)$ are given by $\beta = 2N\omega$, where the weight ω is an $(N-1)$ -tuple formed by eigenvalues of $D(T_q)$ for a simultaneous eigenvector $|\omega\rangle$: $D(T_q)|\omega\rangle = \omega|_q|\omega\rangle$, $q = 1, \dots, N-1$.

which is single-valued when going around any loop. Therefore, when embedded in the lattice, the Abelian and non-Abelian link variables are physically equivalent. Moreover, the flux of the Cartan gauge field is distributed around center-vortex guiding centers γ and γ' (physical lines) on the z -axis, starting/ending at $z = 0$, which carry weights β and β' , respectively. The flux is conserved because of an unobservable Dirac line starting at $z = 0$. Indeed, the Dirac lines are characteristic of the De Grand-Touissant technique [37] used to detect the monopole sector in the above-mentioned lattice studies in the MAG.

4. Monopole worldline matching-rules

In four dimensions, monopole worldlines carrying different adjoint weights can also be matched. For example, when $N \geq 3$, there is a phase $S \in SU(N)$ [18] that represents three open worldsurfaces carrying magnetic weights β , β' , and β'' , attached in pairs to open monopole worldlines carrying charges α_1 , α_2 , and α_3 :

$$\beta - \beta' = 2N\alpha \quad , \quad \beta' - \beta'' = 2N\gamma \quad , \quad \beta'' - \beta = 2N\delta \quad . \quad (5)$$

In this configuration, the three worldlines meet at their initial and final endpoints, thus forming a closed object. This matching is possible because of the condition

$$\alpha + \gamma + \delta = 0 \quad . \quad (6)$$

Of course, there are also higher order configurations involving, say, four monopole worldlines with charges that satisfy

$$\alpha + \gamma + \delta + \sigma = 0 \quad . \quad (7)$$

These possibilities are the lower-dimensional counterpart of the matching of center-vortex worldsurfaces in groups of N , discussed in Sec. II 2.

5. Non Abelian d.o.f.

In Refs. [38–40], a procedure similar to the lattice Laplacian center gauge [41] was implemented in the continuum to induce the partition of the gauge-field configuration space into sectors labeled by singular mappings S . For each label in Eqs. (1)-(4), while S and US describe the same sector, S and $S\tilde{U}^{-1}$ describe physically inequivalent sectors (U and \tilde{U} are regular mappings). As the inequivalent defects are located at the same points in physical space, a continuum of non-Abelian d.o.f. \tilde{U} are implied. These d.o.f. were modelled in center-vortex ensembles [18, 29], where they modify the field content and the symmetries of the effective descriptions. Another related effect could take place at intermediate distances, where the center-vortex thickness cannot be disregarded when compared with the Wilson loop size. Indeed, in this regime, non-Abelian information inherent to center vortices was assumed to reproduce [42, 43] the intermediate Casimir scaling of the confining flux tube [44].

In Secs. II A and II B, we shall discuss how the main ingredients listed above were implemented at the level of the wavefunctional and the partition function, respectively. In both cases, the objective was to obtain effective representations that could capture the confining properties of $SU(N)$ YM theory in asymptotically large Wilson loops, where the center-vortex thickness is only a boundary effect and N -ality properties should be reproduced.

A. The Abelian projected mixed ensemble (wavefunctional)

In the Hamiltonian formalism, the wavefunctional Ψ depends on the gauge field variable $A_i(\mathbf{x})$, $\mathbf{x} \in \mathbb{R}^3$, defined on a given time-slice. At a fixed time, vortex worldsurfaces are simply seen as loops. Center-vortex dominance was then implemented [27] by initially considering a vacuum wavefunctional peaked at Abelian-projected center-vortex gauge fields $a(\{\gamma\})$

$$\Psi(A) = \sum_{\{\gamma\}} \psi_{\{\gamma\}} \delta(A - a(\{\gamma\})) . \quad (8)$$

Here, $a(\{\gamma\})$ is in the Cartan subalgebra of $\mathfrak{su}(N)$ and $\{\gamma\}$ is a particular vortex network $\{\gamma\}$ formed by loops and a given distribution of defining magnetic weights β_i . The amplitude ψ_{γ} parametrizes the center-vortex tension, stiffness, and interactions. We also included the above-mentioned chains, where an elementary vortex line with flux β_i is followed by another with flux β_j . The complete wavefunctional was then written as

$$\Psi(A, \zeta) = \sum_{\{\gamma\}} \psi_{\{\gamma\}} \delta(A - a(\{\gamma\})) \delta(\zeta - (-\Delta)^{-1} \nabla \cdot b(\{\gamma\})) , \quad (9)$$

The monopole potential ζ was included so as to get rid of the unobservable Dirac lines, only keeping the physical information at their endpoints. It allows us to define the variable $\nabla \times A - \nabla \zeta$, which represents the chromomagnetic field of chains. Indeed, in the wavefunctional (9), this variable is localized at the collimated fluxes $b(\{\gamma\})$ of the vortex network $\{\gamma\}$. In the percolating phase, the simplest effective wavefunctional description is done in the dual language. This was achieved by switching from $\Psi(A, \zeta)$ to the electric field representation $\tilde{\Psi}(E, \eta)$ by means of a functional Fourier transform. Polymer techniques were then applied to the center-vortex lines, which gave place to N complex scalar fields ϕ_1, \dots, ϕ_N , corresponding to the possible fluxes β_1, \dots, β_N , respectively. Organizing them as an $N \times N$ diagonal matrix Φ whose entries are the complex scalars ϕ_i , we obtained

$$\begin{aligned} \tilde{\Psi}(E, \eta) &= \int D\Phi e^{-W[\Phi, \Phi^\dagger, \Lambda]} \quad , \quad E = \nabla \times \Lambda \quad , \quad -\nabla^2 \eta = \nabla \cdot \Lambda \quad , \\ W[\Phi, \Phi^\dagger, \Lambda] &= \int d^3x \left(\text{Tr}((D(\Lambda)\Phi^\dagger)D(\Lambda)\Phi) + V(\Phi, \Phi^\dagger) \right) \quad , \\ V(\Phi, \Phi^\dagger) &= \frac{\lambda}{2} \text{Tr}(\Phi^\dagger \Phi - \vartheta^2 I_N)^2 - \xi(\det \Phi + \det \Phi^\dagger) - \nu \text{Tr}(\Phi^\dagger T_A \Phi T_A) . \end{aligned} \quad (10)$$

The parameter λ gives the strength of the repulsive contact interaction among center vortices. In addition, ξ and ν weight the importance of N -matching and the monopole component, respectively. Note that, in the last term, the partial sum over the Cartan sector $A = q$ only redefines the mass parameter, while the off-diagonal contribution is proportional to $\sum_{i \neq j} \bar{\phi}_i \phi_j$. This precisely generates the transitions between center-vortex lines labeled by β_i and β_j , thus introducing center-vortex/monopole chains into the ensemble. The first term is $U(1)^N$ -symmetric. Then, if percolation were the only effect ($\vartheta^2 > 0$), no domain wall could be formed as the vacuum manifold would be $U(1)^N$, which is not discrete. When percolation dominates and N -matching is strong, because of the $\det \Phi$ -term, we considered the most relevant degrees to be on $U(1)^{N-1}$. Finally, we turned on the presence of monopoles to form collimated chains ($\nu \neq 0$), which further reduced the symmetry to $Z(N)$ and the vacua to be discrete, thus leading to confinement through the formation of a domain wall sitting on the Wilson loop. The asymptotic string tension obtained satisfies the Casimir law.

B. Mixed ensemble with non-Abelian d.o.f. (partition function)

In Ref. [18] (see also [23]), we motivated the construction of the 4D partition function for center vortices based on the lattice description of the Abelian ensemble of surfaces given in Ref. [22]. In this reference, a complex-valued field $V(C)$ defined on closed loops C was considered. In particular, it was argued that the loop condensate, where $V(C)$ has frozen modulus, is described by the Abelian Wilson action for link variables $V_\mu(x) \in U(1)$. In other words, the Goldstone modes for a condensate of Abelian loops are given by a $U(1)$ gauge-field. Moreover, the Kalb-Ramond field $b_{\mu\nu}$ coupled to the surfaces manifests as a frustration at the plaquettes given by $e^{ia^2 b_{\mu\nu}}$. Now, in the center-vortex framework, when the linking number between a surface and a Wilson loop is written as an intersection number, the associated Kalb-Ramond field becomes concentrated on an arbitrary surface $S(\mathcal{C}_e)$ whose border is the Wilson loop. In the lattice, when considering elementary center vortices, this corresponds to a frustration $e^{ib(p)}$, where $b(p) = \pm 2\pi k/N$ if p intersects $S(\mathcal{C}_e)$ and it is trivial otherwise. The sign depends on the relative surface orientations and k is the N -ality of the quark representation D . In this manner, we proposed the representation

$$\frac{Z_v^{\text{latt}}[\alpha_p]}{Z_v^{\text{latt}}[0]}, \quad Z_v^{\text{latt}}[\alpha_{\mu\nu}] = \int [\mathcal{D}V_\mu] e^{-S_v^{\text{latt}}(\alpha_p)},$$

$$S_v^{\text{latt}}(\alpha_p) \propto \sum_{\mathbf{x}, \mu < \nu} \text{Re Tr} \left[I - e^{ib(p)} V_\mu(x) V_\nu(x + \hat{\mu}) V_\mu^{-1}(x + \hat{\nu}) V_\nu^{-1}(x) \right], \quad (11)$$

to generate a center-element average when a Wilson loop in representation D is in the presence of an ensemble of percolating and oriented center-vortex worldsurfaces. In Ref. [18], motivated by the possible presence of non-Abelian degrees of freedom (d.o.f.) on center vortices, a starting point based on non-Abelian variables $V_\mu(x) \in SU(N)$ was considered. This way, surfaces can also meet in groups of N at common links forming a closed path (N -matching). In addition, chains were included by means of a “gas” of dual adjoint holonomies. Weighting them with the simplest geometrical properties (tension and stiffness), we obtained the lattice mixed ensemble of center vortices and chains

$$Z_{\text{mix}}^{\text{latt}}[\alpha_p] = \int [\mathcal{D}V_\mu] e^{-S_v^{\text{latt}}(\alpha_p)} \times Z_m, \quad (12)$$

where Z_m is the partition function for the monopole component. The naive continuum limit gave place to an effective $SU(N)$ gauge field Λ_μ that represents the percolating center-vortex worldsurfaces. In addition, the monopole ensemble was integrated by using polymer techniques, which led to minimally coupled interacting adjoint scalar fields. The natural matching rules between the monopole worldlines correspond to Feynman vertices. Finally, this, together with the emergent non-Abelian Goldstone modes Λ_μ , led to a class of effective Yang–Mills–Higgs (YMH) models. Further details about this construction will be provided and clarified in the next sections.

III. MATRIX REPRESENTATION OF SURFACES

We start by reviewing the lattice ensemble of noninteracting closed oriented surfaces s (connected or not) proposed in Ref. [31]²

$$Z_0 = \sum_{\mathcal{S}} N^{\chi(\mathcal{S})} e^{-\sigma A(\mathcal{S})}. \quad (13)$$

² The sum over \mathcal{S} includes all possible orientations.

Here, $A(\mathcal{S})$ and $\chi(\mathcal{S})$ are the area and the Euler characteristic of \mathcal{S} , N is natural, and σ is a tension parameter. This partition function was shown to be equivalent to a model where the variables are $N \times N$ dimensional matrices $V(x, y)$ of complex numbers that live at the links and satisfy $V(y, x) = V^\dagger(x, y)$. More precisely, there is a γ such that

$$Z_0 = \int DV \exp \left(\gamma \sum_p \text{Tr} V(p) - Q_0[V] \right), \quad (14)$$

$$V(p) = V(x, y)V(y, z)V(z, w)V(w, x) \quad , \quad Q_0[V] = \sum_{\{x, y\}} \mathcal{Q}_0(V(x, y)) \quad , \quad \mathcal{Q}_0(V) = \text{Tr} \left(V^\dagger V \right), \quad (15)$$

$$DV = \prod_{\{x, y\}} dV(x, y) \quad , \quad dV(x, y) = \prod_{i, j} \pi^{-1} d[\text{Re} V_{ij}(x, y)] d[\text{Im} V_{ij}(x, y)], \quad (16)$$

where x, y, z, w are the vertices of a plaquette. The plaquettes include both orientations, that is, for every $V(p)$ there is also a variable $V(p') = V^\dagger(p)$. On the other hand, $\{x, y\}$ denotes a nonoriented link. We will see that the partition function Z_0 can also be thought of as an ensemble of noninteracting colored surfaces, where N colors are independently assigned to each vertex. By expanding Eq. (14) in powers of γ , the contribution of F different plaquettes p_1, \dots, p_F is

$$C(p_1, \dots, p_F) = \frac{\gamma^F}{F!} \int DV (\text{Tr} V(p_1) + \dots + \text{Tr} V(p_F))^F e^{-Q_0[V]}. \quad (17)$$

There are F manners to choose a plaquette from the first factor in Eq. (18), $F - 1$ from the second, etc., so that

$$C(p_1, \dots, p_F) = \gamma^F \int DV \text{Tr} V(p_1) \dots \text{Tr} V(p_F) e^{-Q_0[V]}. \quad (18)$$

For the Gaussian measure,

$$\int DV V_{o_1 p_1}(x_1, y_1) \dots V_{o_n p_n}(x_n, y_n) e^{-Q_0[V]} = \sum_{(j_1, \dots, j_n), (k_1, \dots, k_n)} \delta_{o_{j_1} p_{k_1}} \delta_{x_{j_1} y_{k_1}} \delta_{y_{j_1} x_{k_1}} \dots \delta_{o_{j_n} p_{k_n}} \delta_{x_{j_n} y_{k_n}} \delta_{y_{j_n} x_{k_n}}, \quad (19)$$

where $(j_1, \dots, j_n), (k_1, \dots, k_n)$ are permutations of the sequence $(1, \dots, n)$. If there is no manner to group all the links in pairs having the same location but different orientations, then the result is zero. The nontrivial contributions arise when the plaquettes can generate closed oriented surfaces with F faces. Each pairing defines how to move on the surface to follow the orientation and how to assign the colors. In other words, the partition function in Eq. (14) generates the ensemble (a is the lattice spacing)

$$Z_0 = \sum_{\mathcal{S}_c} e^{-\mu_0 A(\mathcal{S}_c)} \quad , \quad \gamma = e^{-\mu_0 a^2} \quad , \quad A(\mathcal{S}) = a^2 F, \quad (20)$$

where \mathcal{S}_c denotes the different oriented colored surfaces. Regarding the distribution of colors, let us initially consider plaquettes p_1, \dots, p_F with single occupation at the common links. This means that there is only one variable of type $V(x, y)$ (and one of type $V(y, x)$). When $N = 1$, $V(x, y)$ is a complex number and the integral

$$\int dV(x, y) |V(x, y)|^2 e^{-|V(x, y)|^2} = 1, \quad (21)$$

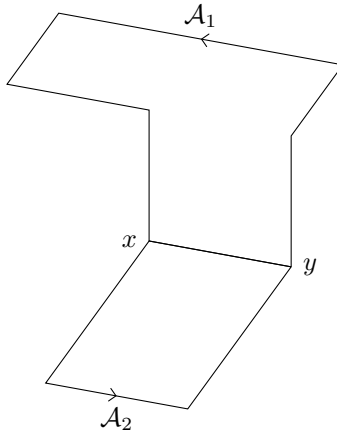


Figure 1: The surfaces $\mathcal{A}_1, \mathcal{A}_2$ with a common link (x, y) .

leads to just one surface. For general N and single occupation, there is still only one orientation induced by the plaquettes that participate in its construction.³ On the other hand, as the contribution originates from products of the form $V_{ij}(x, y)V_{kl}(y, x)$ when $j = k$ and $i = l$, N possible colors are implied at each one of the V vertices:

$$C(p_1, \dots, p_F) = N^V \gamma^F . \quad (22)$$

A. Growing a surface

In order to discuss more general configurations, it is convenient to grow a surface by gluing simpler elements. For this aim, it will be useful to consider the path-ordered product (“holonomy”)

$$\Gamma(\mathcal{C}) = V(x_1, x_2)V(x_2, x_3) \dots , \quad (23)$$

where the links $(x_1, x_2), (x_2, x_3), \dots$ form the curve \mathcal{C} . When two holonomies along closed paths $\partial\mathcal{A}_1, \partial\mathcal{A}_2$ have a common link (x, y) with single occupation and traveled with opposite orientations (see Fig. 1), using

$$\int dV \operatorname{Tr}(VA)\operatorname{Tr}(V^\dagger B) e^{-\mathcal{Q}_0(V)} = \operatorname{Tr}(AB) , \quad (24)$$

we have

$$\int dV(x, y) \operatorname{Tr}(\Gamma(\partial\mathcal{A}_1))\operatorname{Tr}(\Gamma(\partial\mathcal{A}_2)) e^{-\mathcal{Q}_0(V(x, y))} = \operatorname{Tr}(\Gamma(\partial(\mathcal{A}_1 \cup \mathcal{A}_2))) . \quad (25)$$

Then, consider an open surface element formed by n plaquettes glued at links with single occupation that share just one common vertex (see Fig. 2). Using Eq. (25) to integrate one variable shared by p_1, p_2 , one shared by p_2, p_3 , up to one shared by p_{n-1}, p_n , we are left with an integral of the form:

$$\int dV \operatorname{Tr}(VV^\dagger A) e^{-\mathcal{Q}_0(V)} = N \operatorname{Tr}(A) , \quad (26)$$

³ There is also a contribution with the same geometry but different orientation obtained from another term in the expansion containing the adjoint variables.

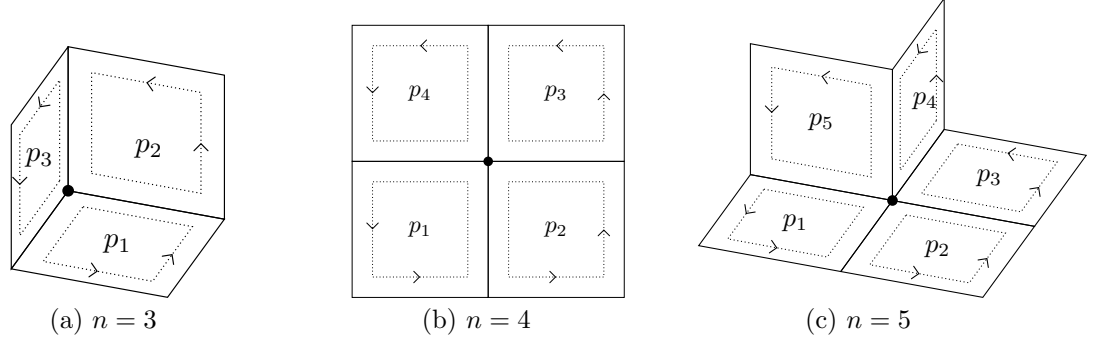


Figure 2: Oriented plaquettes meeting at a common vertex.

computed on the link shared by p_n, p_1 . Thus, the integrals glue the plaquettes and give a partial contribution in terms of the holonomy along the border of the surface element, which contains the nonintegrated variables. This reproduces the factor N for each vertex of s , discussed above:

$$C(p_1, \dots, p_n) = N \text{Tr}(\Gamma(\partial \mathcal{A})) \quad , \quad \mathcal{A} = p_1 \cup \dots \cup p_n . \quad (27)$$

B. A closer look at surfaces in contact

Let us take a closer look at surfaces in contact, which occurs at links with higher occupation. For example, consider configurations generated from F plaquettes p_1, \dots, p_F , with E common links, where E_1 of them have variables with single occupation and the double links are distributed along a curve \mathcal{C} of total size E_2 ($E = E_1 + E_2$). For $N = 1$, the variables at doubly occupied links appear in the form $V^2(x, y)V^2(y, x)$, which yields

$$\int dV (V\bar{V})^2 e^{-|V(x,y)|^2} = 2 \quad , \quad C(p_1, \dots, p_F) = 2^{E_2} e^{-\mu_0 A(\mathcal{S})} . \quad (28)$$

This corresponds to the 2^{E_2} different oriented surfaces that can be constructed out of p_1, \dots, p_F . For general N , each pairing in Eq. (19) defines a choice to glue the oriented plaquettes or, how to move on the surface to follow the orientation. The important point is that the number of vertices and edges of the generated surfaces is generally different from the number of lattice sites and links that participate. Consider an array of four plaquettes p, \bar{p}, q, \bar{q} that meet at a common link (x, y) with double occupation (see Fig. 3a). In the γ -expansion (cf. Eq. (18)), the integration over the variables at (x, y) gives place to two terms (cf. Eq. (A2)). Each one of them is the product of a pair of holonomies along the border of the surface elements $p \cup \bar{p}, q \cup \bar{q}$ and $p \cup \bar{q}, q \cup \bar{p}$ depicted in Figs. 3b and 3c, respectively. In Appendix A, we consider consecutive arrays of this type along \mathcal{C} . For each one of the 2^{E_2} combinations of terms, we have to integrate over the common links to determine the generated surfaces. This allows to visualize whether a given site (link) on \mathcal{C} contains a single vertex (edge) or a pair of superimposed surface vertices (edges). For a given orientation, the number of vertices $V(\mathcal{S})$, edges $E(\mathcal{S})$, and faces $F(\mathcal{S})$ of \mathcal{S} turns out to be

$$V(\mathcal{S}) = V_1 + 2V_2 \quad , \quad E(\mathcal{S}) = E_1 + 2E_2 = 2F \quad , \quad F(\mathcal{S}) = F , \quad (29)$$

where V_1 (V_2) is the number of sites that contribute with a factor N (N^2). That is, there are N possible colors for each vertex of \mathcal{S} . A similar situation applies to higher-order occupations, so that

$$Z_0 = \sum_{\mathcal{S}_c} e^{-\mu_0 A(\mathcal{S}_c)} = \sum_{\mathcal{S}} N^{V(\mathcal{S})} e^{-\mu_0 A(\mathcal{S})} . \quad (30)$$

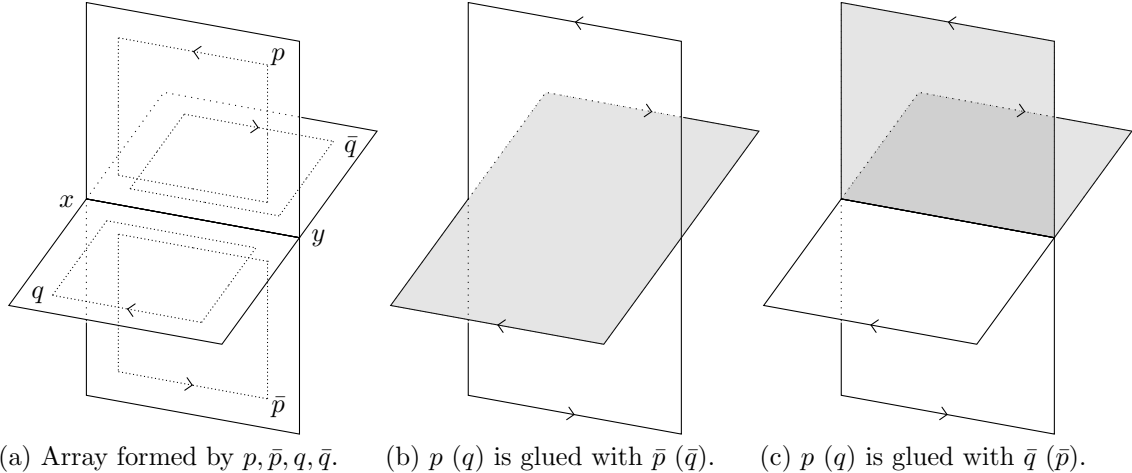


Figure 3: The gluing of four plaquettes: noninteracting and general N case

Note that because of the lattice constraint $E(\mathcal{S}) = 2F$, the degeneracy can be rewritten by redefining the tension and using the Euler characteristic $\chi(\mathcal{S})$ of \mathcal{S} :

$$N^{V(\mathcal{S})}\gamma^F = N^{\chi(\mathcal{S})}e^{-\sigma A(\mathcal{S})} \quad , \quad \sigma = \mu_0 - a^{-2} \ln N \quad , \quad \chi(\mathcal{S}) = V(\mathcal{S}) - E(\mathcal{S}) + F(\mathcal{S}) . \quad (31)$$

This is the content encoded in Eq. (13), which includes all surface types that intersect and/or touch along some curves. Among the orientations, there are disconnected cases where it is not possible to follow the gluing of the plaquettes so as to cover the whole surface. Then, the partition function for noninteracting surfaces can also be cast in the form [45]

$$Z_0 = e^{W_0} \quad , \quad W_0 = \sum_{\mathcal{S} \in \{S_{\text{conn}}\}} N^{\chi(\mathcal{S})} e^{-\sigma A(\mathcal{S})} , \quad (32)$$

where the sum is over the set of connected oriented surfaces, for which the genus $g(\mathcal{S}) = (2 - \chi(\mathcal{S}))/2$ can also be used.

IV. THE GOLDSTONE MODES FOR PERCOLATING SURFACES

As discussed in Ref. [31], even in a finite lattice with periodic boundary conditions, the model defined by Eq. (14) is pathological, as the integral over the link variables gives a divergent Z_0 . In that reference, sixth-order or higher-order interaction terms were proposed to stabilize the model. Its stabilization with a quartic term is also possible. Indeed, the Von Neumann trace inequality,

$$|\text{Tr}(AB)| \leq \sum_{i=1}^N \sigma_i(A)\sigma_i(B) , \quad (33)$$

where $\sigma_1 \geq \sigma_2 \geq \dots \geq \sigma_N$ are the singular values of an $N \times N$ complex matrix, leads to

$$|\text{Tr}(AB)| \leq \frac{1}{2} \sum_{i=1}^N (\sigma_i^2(A) + \sigma_i^2(B)) = \frac{1}{2} \text{Tr}(A^\dagger A + B^\dagger B) . \quad (34)$$

For a generic plaquette $V(p) = ABCD$, this implies

$$\begin{aligned} \text{Tr}V(p) &\leq |\text{Tr}V(p)| \leq \frac{1}{2}\text{Tr}((AB)^\dagger(AB) + (CD)^\dagger(CD)) \\ &= \frac{1}{2}\text{Tr}(A^\dagger ABB^\dagger) + \frac{1}{2}\text{Tr}(C^\dagger CDD^\dagger) \\ &\leq \frac{1}{4}\text{Tr}((A^\dagger A)^2 + (B^\dagger B)^2 + (C^\dagger C)^2 + (D^\dagger D)^2). \end{aligned} \quad (35)$$

Note that starting from a given p in Eq. (35) and summing over the oriented plaquettes of the lattice that are in the same plane, each nonoriented link appears four times. As a given link can be in 3 different planes, we get the following bound

$$\sum_p \text{Tr}V(p) \leq 3 \sum_{\{x,y\}} \text{Tr}(V^\dagger(x,y)V(x,y))^2. \quad (36)$$

Therefore, let us consider the quartic model (n_l is the total number of links)

$$Z = \frac{1}{\mathcal{N}(\lambda)} \int DV \exp\left(\gamma \sum_p \text{Tr}V(p) - Q[V]\right), \quad \mathcal{N}(\lambda) = z^{n_l}, \quad (37)$$

$$Q[V] = \sum_{\{x,y\}} Q(V(x,y)) \quad , \quad Q(V) = \text{Tr}\left(\eta V^\dagger V + \lambda(V^\dagger V)^2\right) \quad , \quad z = \int dV e^{-Q(V)}. \quad (38)$$

The factor $\mathcal{N}(\lambda)$ guarantees that, in the γ -expansion, all the links that do not participate in a given surface lead to a trivial contribution. Because of Eq. (36), the partition function Z , where all the link variables are correlated, is bounded by an uncorrelated integral:

$$Z \leq \frac{\mathcal{N}(\lambda')}{\mathcal{N}(\lambda)} \quad , \quad \lambda' = \lambda - 3\gamma. \quad (39)$$

Then, in the region $\lambda > 3\gamma$, the model is no longer pathological. For single occupation, the only change is a factor α in the right-hand side of Eqs. (24)-(26)

$$\alpha = \frac{1}{zN^2} \int dV \text{Tr}(VV^\dagger) e^{-Q(V)}. \quad (40)$$

In this case, F plaquettes leading to surfaces with V vertices and E edges yield

$$C(p_1, \dots, p_F) = N^V \gamma^F \alpha^E = N^V e^{-\mu A(S)} \quad , \quad e^{-\mu a^2} = \gamma \alpha^2, \quad (41)$$

that is, the tension is renormalized. Now, as is well known, the Weingarten model for surfaces does not correspond to a field theory [45]. However, this applies to the normal phase. As we shall see, this situation changes in the percolating phase. In effect, after adding and subtracting the bound (36) in the exponent of Eq. (37), we can also write the partition function in the form

$$Z = \frac{1}{\mathcal{N}} \int DV \exp(-S[V]) \quad , \quad S[V] = K[V] + U[V], \quad (42)$$

$$K[V] = 3\gamma \sum_{\{x,y\}} \text{Tr}(V^\dagger(x,y)V(x,y))^2 - \gamma \sum_p \text{Tr}V(p),$$

$$U[V] = \lambda' \sum_{\{x,y\}} \text{Tr}(V^\dagger(x,y)V(x,y) - \vartheta^2 I)^2 + c \quad , \quad \vartheta^2 = \frac{-\eta}{2\lambda'} \quad , \quad c = -\lambda' N \vartheta^4 n_l. \quad (43)$$

By construction, $K[V]$ is positive definite. This also applies to the squared terms in $U[V]$. In Fig. 4, we see that when the renormalized tension is below a critical value $\mu_c > 0$ (percolating surfaces), the parameter η becomes negative, thus leading to a transition where ϑ^2 becomes positive. The absolute minima of $S[V]$ are those minima of $U[V]$ that nullify $K[V]$. The former condition means

$$V(x, y) = \vartheta U(x, y) \quad , \quad U(x, y) \in U(N) . \quad (44)$$

At these minima, in order for $K[V]$ to be zero, the bound (35) must be saturated for every plaquette. Then, at the absolute minima, all the plaquette variables $U(p)$ formed out of the link variables $U(x, y)$ must be trivial. That is, $U(x, y)$ must be pure gauge. Now, in the thermodynamic limit, a condensate dominated by the ‘‘Goldstone’’ modes in Eq. (44) is expected to be formed, accompanied by massive fluctuations away from the minima of the potential, with ‘‘mass’’ $\lambda'\vartheta^2$. In the case where λ' is much larger than γ , the massive modes get suppressed, we can freeze the ‘‘modulus’’ of $V(x, y)$, and keep the softer Goldstone modes governed by $K[V]$:

$$Z \approx \frac{1}{N} \int DU e^{-K[U]} \quad , \quad K[U] \approx \gamma\vartheta^2 \sum_p \text{Tr}(I - U(p)) . \quad (45)$$

This is nothing but the Wilson action for the $U(N)$ gauge field theory. The representation of a condensate of Abelian loops in terms of Abelian gauge Goldstone modes was done for the first time in Ref. [22]. Here, relying on the Weingarten representation, this result was generalized to percolating oriented surfaces with N possible colors at their vertices. Note that, when $\vartheta^2 > 0$ and $\lambda \rightarrow \infty$, the non-Gaussian integral with measure dV in Eq. (38) becomes a group integral over $U(N)$ with Haar measure $d\mu(U)$:

$$\int dV z^{-1} \exp(-\mathcal{Q}(V)) f(V) = \int d\mu(U) f(\vartheta U) . \quad (46)$$

Then, when $\lambda \rightarrow \infty$, the approximation in Eq. (45) becomes exact.

Regarding the interaction properties of the ensemble, we can look at the effect of doubly occupied links. For $N = 1$, we have

$$\frac{\int dV (V\bar{V})^2 e^{-\mathcal{Q}(V)}}{\int dV e^{-\mathcal{Q}(V)}} = 2\beta > 0 \quad , \quad C(p_1, \dots, p_F) = 2^{E_2} e^{-\mu A(S)} e^{-\xi L(C)} \quad , \quad e^{-\xi a} = \frac{\beta}{\alpha^2} , \quad (47)$$

where $L(C) = aE_2$ is the length of the curve \mathcal{C} where the surfaces are in contact. In Fig. 5, we see that the interaction between the surfaces is repulsive ($\xi > 0$) in the normal as well as in the percolating phase. Then, in the Abelian case, besides excluded volume effects, the quartic interaction also provides some stiffness. In particular, a strong repulsion prevents a surface from bending at angles of 180 degrees, which tends to prevent crumpling. For a general analysis of the importance of stiffness to stabilize random surfaces, see Ref. [46]. In the non-Abelian case ($N \geq 2$), interpreting the effect of the quartic term in Eq. (38) on the ensemble is a difficult task. For instance, when considering the four-plaquette array in Fig. 3a, the gluings in Figs. 3b and 3c gain a factor β_a (see Appendix A). In addition, two new terms with a factor β_b are generated. They are given by a holonomy along the path $\partial(p \cup \bar{p})$ composed with $\partial(q \cup \bar{q})$ and the path $\partial(p \cup \bar{q})$ composed with $\partial(q \cup \bar{p})$, which define the border of new surface elements. In particular, for a surface which along \mathcal{C} is formed by a given sequence of m (n) surface elements of type a (b), the contribution is ($E_1 + 2E_2 = 2F$, $E_2 = m + n$)

$$N^{V(S)} e^{-\mu A(S)} \left(\frac{\beta_a}{\alpha^2} \right)^m \left(\frac{\beta_b}{\alpha^2} \right)^n . \quad (48)$$

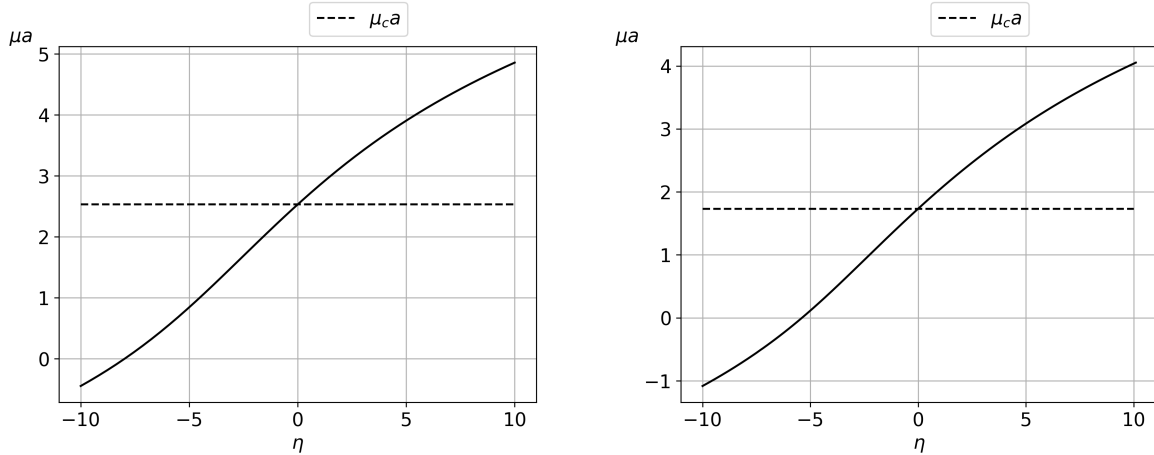


Figure 4: The renormalized tension μ as a function of η for $\lambda = 4, \gamma = 1$. When $\mu < \mu_c$, a condensate is formed ($\eta < 0$). This is shown for $N = 1$ (left) and $N = 3$ (right).

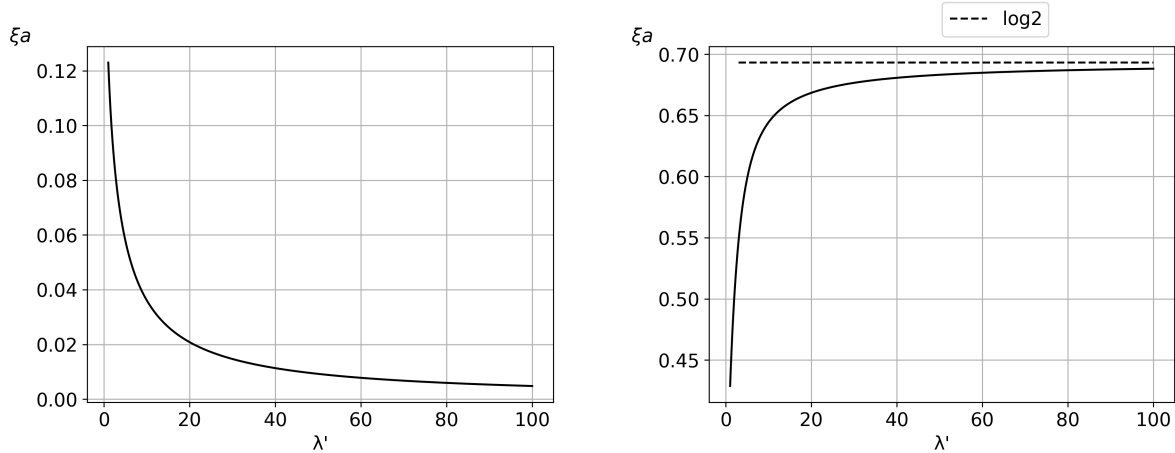


Figure 5: For $N = 1$ and $\lambda' > 0$ there is repulsion between surfaces: the interaction strength ξ is positive in the normal $\vartheta^2 = -1$ phase (left) and in the percolating $\vartheta^2 = 1$ phase (right).

Then, new combinations are generated with respect to the noninteracting Weingarten model, which increase for higher occupation. Over the years, numerous efforts have been made to interpret non-Abelian lattice models in terms of surfaces. Historically, these attempts were mainly concerned with determining a reference point where fundamental strings are free. For this reason, the focus was on implementing the 't Hooft large N -limit [47] in lattice theories directly associated to the non-Abelian interactions. For instance, a thorough analysis aimed at establishing a link between the large- N limit of $U(N)$ lattice gauge theory and strings was given in Refs. [48]-[50]. Also, a matrix model formed by the terms in Eq. (38), nonlocal Coulomb interactions, and additional quartic terms, was considered in the large- N limit to describe free Nambu-Goto strings [51] and to study bound states in pure YM theory [52]. In our work, the matrix model is also aimed at describing the strong interactions, but through the modeling of percolating center-vortex worldsheets. The ensemble interpretation can be given at the end, as its behavior will be essentially Abelianized due to the inclusion of chains and other relevant correlations observed in $SU(N)$ YM theory at finite N . Confining strings will also appear later, as topological solitonic flux tubes in the effective field descriptions.

V. ENSEMBLES OF LOOPS IN THE LATTICE

In Ref. [18], the ensemble of holonomies along the monopole worldlines was treated as the continuum limit of a polymer growth process with stiffness. In the next sections, we will need an ensemble representation in the same language used for surfaces. Then, let us briefly discuss the Weingarten representation of loops (for the Abelian case, see [45]). Similarly to Eqs. (37), (38), consider the partition function

$$Z_m[R] = \frac{1}{\tilde{\mathcal{N}}} \int D\zeta \exp \left(\sum_l \tilde{V}(l) - \tilde{Q}[\zeta] \right) \quad , \quad \tilde{V}(l) = \zeta^\dagger(x) H(x, y) \zeta(y) \quad , \quad (49)$$

$$\tilde{Q}[\zeta] = \sum_x \tilde{Q}(\zeta(x)) \quad , \quad \tilde{Q}(\zeta) = \tilde{\eta} \zeta^\dagger \zeta + \tilde{\lambda} (\zeta^\dagger \zeta)^2 \quad , \quad \tilde{\mathcal{N}} = \int D\zeta e^{-\tilde{Q}[\zeta]} \quad , \quad (50)$$

$$D\zeta = \prod_x d\zeta(x) \quad , \quad d\zeta(x) = \prod_A \pi^{-1} d[\text{Re } \zeta_A(x)] d[\text{Im } \zeta_A(x)] \quad , \quad (51)$$

where the sum is over the oriented links $l = (x, y)$ and the source satisfies $H(y, x) = H(x, y)^\dagger$. The tuple ζ is defined at the sites and is formed by \mathcal{D} complex components, while $R(x, y)$ is a $\mathcal{D} \times \mathcal{D}$ matrix. In the \tilde{V} -expansion, the contribution of sites with single occupation is distributed on loops $\mathcal{C}_1, \mathcal{C}_2, \dots$, and is proportional to products of loop-variables

$$\text{Tr } H(x_1, x_2) \dots H(x_n, x_1) \quad , \quad (52)$$

where $(x_1, x_2), \dots, (x_n, x_1)$ are the n links forming \mathcal{C} . For example, if

$$H(x, y) = \tilde{\gamma} R(x, y) \quad , \quad R^\dagger(x, y) R(x, y) = I_{\mathcal{D}} \quad , \quad (53)$$

this contribution is given in terms of group holonomies $\Gamma_R(\mathcal{C})$:

$$e^{-\tilde{\mu}(L(\mathcal{C}_1)+L(\mathcal{C}_2)+\dots)} \text{Tr } \Gamma_R(\mathcal{C}_1) \text{Tr } \Gamma_R(\mathcal{C}_2) \dots \quad , \quad \Gamma_R(\mathcal{C}) = R(x_1, x_2) \dots R(x_n, x_1) \quad , \quad (54)$$

$$\tilde{\gamma} \tilde{\alpha} = e^{-\tilde{\mu}a} \quad , \quad L(\mathcal{C}) = na \quad , \quad \tilde{\alpha} = \frac{1}{\mathcal{D}} \int d\zeta (\zeta^\dagger \zeta) e^{-\tilde{Q}(\zeta)} \quad . \quad (55)$$

In this case, we can rewrite

$$-\sum_l \tilde{V}(l) + \tilde{Q}[\zeta] = \tilde{\gamma} \sum_{x, \mu} (\Delta_\mu \zeta)^\dagger \Delta_\mu \zeta + \sum_x \left(a^2 m^2 \zeta^\dagger \zeta + \tilde{\lambda} (\zeta^\dagger \zeta)^2 \right) \quad , \quad (56)$$

$$\Delta_\mu \zeta = R(x, x + \mu) \zeta(x + \mu) - \zeta(x) \quad , \quad \tilde{\eta} = 2d\tilde{\gamma} + a^2 m^2 \quad ,$$

where d is the spacetime dimension ($d = 4$ in our case). In general, m^2 controls whether the model displays SSB or not. As is well-known, when the tension $\tilde{\mu}$ goes below a critical value $\tilde{\mu}_c > 0$, a condensate is formed ($m^2 < 0$). That is, bosons with sufficiently small mass and repulsive interactions condense. The condensation of loops spanning surfaces, discussed in the previous section, is the higher dimensional version of this property. Furthermore, if we redefine $\zeta(x) \rightarrow a \zeta(x)$, Eq. (56) is the discretized action for the complex scalar ζ :

$$\int d^4x \left((\tilde{\gamma} (D_\mu \zeta)^\dagger D_\mu \zeta + m^2 \zeta^\dagger \zeta + \tilde{\lambda} (\zeta^\dagger \zeta)^2 \right) \quad . \quad (57)$$

VI. ABELIAN PROJECTED ENSEMBLES

In what follows, we shall obtain the 4D partition function for the ensemble represented by the vacuum wavefunctional reviewed in Sec. II A.

A. Abelian projected center vortices

To arrive at the wavefunctional in Eq. (10), we initially considered elementary center-vortex loops (see Sec. II 1), that is, their center charge is ± 1 . As already discussed, there are N species labeled by the (magnetic) weights of the defining representation β_i . In Euclidean spacetime, the loops generate worldsheets \mathcal{S} (guiding centers) labeled by these weights. As the different species are physically equivalent, the possible ensembles must be invariant under permutations of β_i (Weyl transformations). Therefore, in the Abelian projected case, it is clear that the partition function for center-vortex “matter” will be constructed in terms of N copies of the Weingarten model for a single complex link variable. Each variable $V_i \in \mathbb{C}$, $i = 1, \dots, N$, will generate surfaces with a global magnetic charge β_i . On the other hand, in the continuum, for heavy quark probes in an irreducible representation $D(\cdot)$, with dimensionality \mathcal{D} , the Wilson loop for Cartan gauge fields A_μ is given by:

$$\mathcal{W}_D(\mathcal{C}_e) = \frac{1}{\mathcal{D}} \text{Tr} D \left(e^{i \int_{\mathcal{C}_e} dx_\mu A_\mu(x)} \right) = \frac{1}{\mathcal{D}} \sum_{\omega_D} e^{i \int d^4x (\mathcal{F}_{\mu\nu}, \omega_D \cdot T) s_{\mu\nu}} , \quad (58)$$

where ω_D are the weights of $D(\cdot)$ and $s_{\mu\nu}$ is localized on a surface $\mathcal{S}(\mathcal{C}_e)$ whose border is \mathcal{C}_e :

$$s_{\mu\nu} = \int_{\mathcal{S}(\mathcal{C}_e)} d^2 \tilde{\tau}_{\mu\nu} \delta^{(4)}(x - \bar{x}(\tau_1, \tau_2)) \quad , \quad \mathcal{F}_{\mu\nu} = \frac{1}{2} \epsilon_{\mu\nu\rho\sigma} F_{\rho\sigma} . \quad (59)$$

The scalar product (X, Y) between Lie algebra elements follows the conventions of Ref. [26]. Now, when the distance between the guiding centers \mathcal{S} and \mathcal{C}_e is larger than the thickness a_c of a center vortex, the holonomy gives a center-element

$$D \left(e^{i \int_{\mathcal{C}_e} dx_\mu A_\mu(x)} \right) = e^{-i \frac{2\pi k}{N} L(\mathcal{S}, \mathcal{C}_e)} I_{\mathcal{D}} , \quad (60)$$

where k determines how the center of $SU(N)$ is realized in $D(\cdot)$ (N -ality), and $L(\mathcal{S}, \mathcal{C}_e)$ is the linking number between \mathcal{S} and \mathcal{C}_e . For example, when an elementary center vortex is linked by \mathcal{C}_e once, Eq. (60) computed for the gauge field a_μ in Eq. (2) gives $(\Delta\chi = 2\pi)$

$$D \left(e^{i 2\pi \beta_i \cdot T} \right) = D \left(e^{-i \frac{2\pi}{N} I} \right) = e^{-i \frac{2\pi k}{N} I_{\mathcal{D}}} . \quad (61)$$

For asymptotically large \mathcal{C}_e compared with a_c , the effect of center-vortex thickness on $\langle \mathcal{W}_D(\mathcal{C}_e) \rangle$ only scales as its perimeter. In this regime, we shall disregard the effect at the boundary by considering Eq. (60) for every center vortex. The linking number can also be written as an intersection number:

$$e^{-i \frac{2\pi k}{N} L(\mathcal{S}, \mathcal{C}_e)} = e^{-i \int_{\mathcal{S}} d^2 \sigma_{\mu\nu} b_{\mu\nu}} \quad , \quad b_{\mu\nu} = (2\pi k/N) s_{\mu\nu} , \quad (62)$$

In the noninteracting case, the center-element average over worldsheets \mathcal{S} only characterized by its orientation and a given global weight would be

$$\sum_{\mathcal{S}} e^{-\mu_0 A(\mathcal{S}) - i \int_{\mathcal{S}} d^2 \sigma_{\mu\nu} b_{\mu\nu}} . \quad (63)$$

The sum over surfaces can be regularized in the lattice, where the Weingarten representation gives

$$Z_0[b] = \int DV \exp \left(\gamma \sum_p e^{ib(p)} V(p) - Q_0[V] \right) \quad , \quad V \in \mathbb{C} . \quad (64)$$

If the source $b_{\mu\nu}$ were smooth, the frustration would be $b(p) = a^2 b_{\mu\nu}$ (see Refs. [22], [45]). For the Wilson loop, we have $b(p) = (2\pi k/N) s(p)$, where $s(p)$ equals $+1$ (-1) if the relative orientation between p and \mathcal{S}_{C_e} at the intersection point is positive (negative). This ensemble can be stabilized by excluded volume effects and stiffness at 180 degrees. Then, in the Abelian projected scenario, the average of the Wilson loop over the N worldsurface types, with global charges β_i , is given by the partition function for N complex fields V_i (cf. Eq. (38)):

$$(Z[b])^N = \frac{1}{\mathcal{M}} \int \int \prod_i DV_i \exp \left(\gamma \sum_p \text{Tr}(e^{ib(p)} V(p)) - Q[V] \right) , \quad (65)$$

where we introduced a diagonal $N \times N$ matrix V :

$$V = \begin{pmatrix} V_1 & 0 & \cdots & 0 \\ 0 & V_2 & \cdots & 0 \\ \vdots & \vdots & \ddots & \vdots \\ 0 & 0 & \cdots & V_N \end{pmatrix} . \quad (66)$$

Note that $Q[V]$ in Eq. (65) is given by Eq. (38) but applied to this $N \times N$ diagonal matrix. Up to this point, the model displays a $U(1)^N$ local symmetry

$$V(x, y) \rightarrow U(x)V(x, y)U^\dagger(y) \quad , \quad U(x) \in U(1)^N . \quad (67)$$

Now, similarly to the wavefunctional in Eq. (10), the natural N -matching among vortices discussed in Sec. II 2 can be simply implemented by

$$\begin{aligned} Z_{\text{c.v.}}[b] &= \frac{1}{\mathcal{M}} \int DV \exp(-W_{\text{c.v.}}[V]) \quad , \quad DV = DV_1 \dots DV_N , \\ W_{\text{c.v.}}[V] &= -\gamma \sum_p \text{Tr}(e^{ib(p)} V(p)) + Q[V] - \sum_{\{x,y\}} \xi (\det V(x, y) + \det V(y, x)) . \end{aligned} \quad (68)$$

Indeed, upon expanding in powers of ξ and γ , the only nontrivial contributions arise from terms where all variables are paired. The new term $\xi V_1(x, y) \dots V_N(x, y)$ allows for the possibility of having N open surfaces carrying the weights β_1, \dots, β_N ($\beta_1 + \dots + \beta_N = 0$) that meet at links (x, y) that form loops. With this N -matching property, the local symmetry is reduced to $U(1)^{N-1}$:

$$V(x, y) \rightarrow U(x)V(x, y)U^\dagger(y) \quad , \quad U(x) = e^{i\xi(x) \cdot T} . \quad (69)$$

B. Abelian projected chains

Here, in the context of the Weingarten representation, we shall include the chains discussed in Sec. II 3. This can be easily done by including a factor $Z_m[H]$ that generates loops (cf. Eq. (49)) in the integrand of Eq. (68), which generates surfaces:

$$\begin{aligned} Z_{\text{mix}}[b] &\propto \int DV D\phi \exp(-W_{\text{mix}}[V, \phi]) \quad , \quad W_{\text{mix}}[V, \phi] = W_{\text{c.v.}}[V] - \sum_l \tilde{V}(l) + \tilde{Q}[\phi] , \\ \tilde{V}(l) &= \sum_\alpha \bar{\phi}_\alpha(x) H_\alpha(x, y) \phi_\alpha(y) \quad , \quad H_\alpha(x, y) = \bar{V}_j(x, y) V_i(x, y) , \\ \tilde{Q}[\phi] &= \sum_x \sum_\alpha \tilde{\mathcal{Q}}(\phi_\alpha(x)) \quad , \quad \tilde{\mathcal{Q}}(\phi) = \bar{\eta} \bar{\phi} \phi + \tilde{\lambda} (\bar{\phi} \phi)^2 . \end{aligned} \quad (70)$$

Here, α is a shorthand notation for the pair of indices ij , $i < j$. Note that when expanding in powers of \tilde{V} , products of loop variables (cf. Eq. (52))

$$H_\alpha(x_1, x_2) \dots H_\alpha(x_n, x_1) = V_i(x_1, x_2) \dots V_i(x_n, x_1) V_j(x_1, x_n) \dots V_j(x_2, x_1) ,$$

with the different α combinations, are generated. Thus, in the γ -expansion, plaquettes of type i can be glued to type j along \mathcal{C} . That is, we gain chains where an open center-vortex worldsurface with global charge β_i can be transformed into another with global charge β_j at a monopole worldline. Because of the frustration, center elements that depend on the linking number between chains and \mathcal{C}_e will also be present. This agrees with the Wilson loop calculation, based on a non-Abelian gauge field labeled by S in Eq. (4), when the cores are completely linked by \mathcal{C}_e . The mixed model continues to display a local $U(1)^{N-1}$ symmetry (cf. Eq. (67)), which also transforms the monopole fields

$$V_i(x, y) \rightarrow e^{i\xi(x)\cdot\omega_i} V_i(x, y) e^{-i\xi(y)\cdot\omega_i} \quad , \quad \phi_\alpha(x) \rightarrow e^{i\xi(x)\cdot\alpha_{ij}} \phi_\alpha(x) \quad , \quad \alpha_{ij} = \omega_i - \omega_j . \quad (71)$$

Since α_{ij} is a difference of defining weights, the label α can be identified with a (positive) weight of the adjoint representation of $\mathfrak{su}(N)$.

C. Percolating phase

Now, we recall that in the wavefunctional approach to the mixed ensemble, there is a physically interesting sequence of phase transitions. Initially, we considered the formation of a center-vortex condensate, where N -matching forces the vortex field Φ in Eq. (10) to be in $U(1)^{N-1}$. This was followed by a softer transition where monopoles are turned on. Let us consider the same process in the language of the 4D partition function $Z_{\text{mix}}[b]$. From the discussion in Sec. IV, when center-vortex worldsheets percolate and have repulsive interactions ($\eta < 0$, $\lambda' = \lambda - 3\gamma > 0$), $Q[V]$ in Eq. (68) drives the matrix $V(x, y)$ in Eq. (66) to be close to $\vartheta U(x, y)$, $U(x, y) \in U(1)^N$ (see the discussion that led to Eq. (45)). In addition, for a large ξ , the determinant favors N -matching and forces $U(x, y)$ to be close to $U(1)^{N-1}$:

$$U(x, y) = e^{i\theta(x,y)\cdot T} \quad , \quad U_i(x, y) = e^{i\theta(x,y)\cdot\omega_i} . \quad (72)$$

If this initial stage dominates, for $\alpha = \alpha_{ij}$, we obtain

$$H_\alpha(x, y) = \vartheta^2 R_\alpha(x, y) \quad , \quad R_\alpha(x, y) = U_i(x, y) \bar{U}_j(x, y) = e^{i\theta(x,y)\cdot\alpha} . \quad (73)$$

Therefore, when center vortices percolate, we may use Eq. (56) to approximate the mixed ensemble model:

$$W_{\text{mix}}[V, \phi] \approx \gamma \vartheta^2 \sum_p \text{Tr} \left(I - e^{ib(p)} U(p) \right) + \sum_{x, \mu, \alpha} \vartheta^2 (\Delta_\mu \phi_\alpha)^\dagger \Delta_\mu \phi_\alpha + \mathcal{U}(\phi) ,$$

$$\Delta_\mu \phi_\alpha = R_\alpha(x, x + \mu) \phi_\alpha(x + \mu) - \phi_\alpha(x) \quad , \quad \mathcal{U}(\phi) = \sum_{x, \alpha} (a^2 m^2 |\phi_\alpha|^2 + \tilde{\lambda} |\phi_\alpha|^4) . \quad (74)$$

As in previous works, besides the center-vortex condensate we shall also assume a monopole condensate ($m^2 < 0$). After disregarding boundary effects, the only information left about the initial quark representation $D(\cdot)$ is k , so that asymptotic N -ality is explicitly implemented. In particular, for adjoint quarks, there is no frustration at all and the Wilson loop average gives just 1 (no confining string).

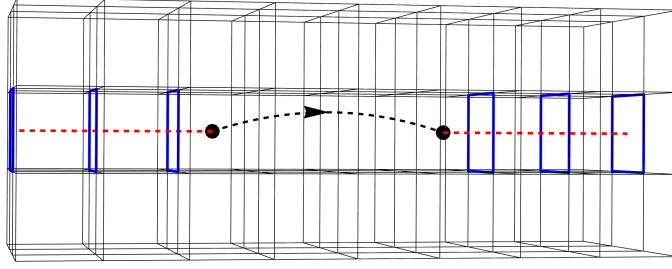


Figure 6: At an intermediate time-slice ($x_0 = 0$), we see a quark-antiquark pair (black dots) that belongs to the Wilson loop \mathcal{C}_e . The dotted red lines belong to $S(\mathcal{C}_e)$, while the black lines represent the observable guiding centers of the flux tube. The plaquettes \tilde{p} that intersect $S(\mathcal{C}_e)$ are in blue.

D. Abelian projection and the confining flux tube

For nontrivial k , let us initially consider a Wilson loop along a large (compared with a_c) rectangular path \mathcal{C}_e in the x_0, x_3 plane. The frustration can be assigned to the plaquettes that intersect any surface whose border is \mathcal{C}_e . For definiteness, let us consider the surface $|x_0| > T/2$, $|x_1| > R/2$, $x_2 = 0$, $x_3 = 0$. At an intermediate time-slice ($x_0 = 0$), we have a cubic lattice in \mathbb{R}^3 (Fig. 6). The cubes centered at $x_1 = \pm L/2$, $x_2 = 0$, $x_3 = 0$ contain the quark and antiquark. The partition function $Z_{\text{mix}}[b]$ will be dominated by the lowest action configurations of $W_{\text{mix}}[V, \phi]$, which could be directly obtained from computer lattice calculations. To gain insight about them, we note that at large distances from the quark and antiquark, they should be close to

$$U(p) = e^{-ib(p)} I \quad , \quad R_\alpha(x, y) \phi_\alpha(y) = \phi_\alpha(x) \quad , \quad \bar{\phi}_\alpha \phi_\alpha = v^2 \quad , \quad (75)$$

where $v^2 = -a^2 m^2 / (2\tilde{\lambda})$. This gives (cf. Eq. (73))

$$U(l) = e^{i\Delta(l) \cdot T} \quad , \quad e^{i\sum_{l \in \partial p} \Delta(l) \cdot T} = e^{-ib(p)} I \quad , \quad e^{i\Delta(l) \cdot \alpha} \phi_\alpha(y) = \phi_\alpha(x) \quad , \quad (76)$$

where $l = (x, y)$. In particular, at nontrivial plaquettes \tilde{p} with positive orientation relative to $S(\mathcal{C}_e)$,

$$e^{i\sum_{l \in \partial \tilde{p}} \Delta(l) \cdot T} = e^{-i\frac{2\pi k}{N}} I \quad . \quad (77)$$

Indeed, when $a \rightarrow 0$, Eq. (77) will be satisfied at every plaquette \tilde{p} with nontrivial frustration. This is because $b(p)$ does not scale as a^2 , so its effect, concentrated on a surface, would produce a divergent action. To solve these conditions, note that Eq. (61) is valid for any representation $D'(\cdot)$ of $SU(N)$ with N -ality k . Using

$$D' \left(e^{i2\pi \beta_i \cdot T} \right) = e^{i2\pi \beta_i \cdot D'(T)}$$

and acting on any weight-vector of $D'(\cdot)$ with weight ω' , we have $e^{i2\pi \beta_i \cdot \omega'} = e^{-i2\pi k/N}$. Equivalently,

$$e^{i2\pi \beta' \cdot T} = e^{-i\frac{2\pi k}{N}} I \quad , \quad \beta' = 2N\omega' \quad . \quad (78)$$

On the other hand, the nontrivial plaquettes at $x_0 = 0$, are those that intersect the x_1 -axis for $|x_1| > L/2$. Then, away from the quark probes, as the continuum limit is approached, the low-action lattice modes are expected to be close to

$$\Delta(l) = \beta' \Delta_l \xi \quad . \quad (79)$$

Here, ξ is a multivalued phase that changes by 2π when going around a path γ formed by the red and black dotted lines in Fig. 6. This object, defined in the continuum, is embedded in the lattice through its variation $\Delta_l \xi$ along l , which is a well-defined link-variable. In this manner, $\sum_{l \in \partial p} \Delta(l)$ gives $2\pi\beta'$ or 0, depending on whether ∂p links γ or not, which implies the second condition in Eq. (76). Moreover, Eq. (79) leads to well-defined monopole fields: starting from a site x and transforming $\phi_\alpha(x)$ along $\partial \tilde{p}$, due to the third condition we return to $\phi_\alpha(x)$:

$$e^{i2\pi\beta' \cdot \alpha} \phi_\alpha(x) = e^{i2\pi\beta' \cdot \omega_i} e^{-i2\pi\beta' \cdot \omega_j} \phi_\alpha(x) = \phi_\alpha(x) . \quad (80)$$

Now, the key question is which configuration has the lowest action. Of course, a lower action will be obtained by considering a straight line between the quark and the antiquark. But what about the magnetic weight β' , with N -ality k , that must be used? This can be answered by considering the continuum limit of the lattice field equations. By using $\theta(x, y) = a\Lambda_\mu(x)$ in Eqs. (72), (73) and the redefinition $\phi_\alpha \rightarrow a\phi_\alpha$, these equations become

$$\begin{aligned} D^2 \phi_\alpha &= m^2 \phi_\alpha + 2\tilde{\lambda} \phi_\alpha (\bar{\phi}_\alpha \phi_\alpha) \quad , \quad D_\mu = \partial_\mu - i\Lambda_\mu \cdot \alpha \quad , \\ \partial_\nu F_{\mu\nu} &= \gamma \vartheta^2 \sum_\alpha \left(-i(\partial_\mu \bar{\phi}_\alpha \phi_\alpha - \bar{\phi}_\alpha \partial_\mu \phi_\alpha) + 2\Lambda_\mu \cdot \alpha \bar{\phi}_\alpha \phi_\alpha \right) \alpha \cdot T \quad , \quad F_{\mu\nu} = \partial_\mu \Lambda_\nu - \partial_\nu \Lambda_\mu \quad , \end{aligned} \quad (81)$$

while the conditions away from the quark probes are

$$\Lambda_\mu \rightarrow \beta' \cdot T \partial_\mu \xi \quad , \quad \phi_\alpha(\rho) \rightarrow v e^{i\beta' \cdot \alpha \xi} . \quad (82)$$

The corresponding action will be

$$\begin{aligned} S(J') &= \int d^4x \left[\frac{\gamma \vartheta^2}{4} (F_{\mu\nu} - J'_{\mu\nu})^2 + \sum_\alpha D_\mu \bar{\phi}_\alpha D_\mu \phi_\alpha + \mathcal{U}(\phi) \right] \quad , \quad \mathcal{U}(\phi) = \sum_\alpha \left(m^2 |\phi_\alpha|^2 + \tilde{\lambda} |\phi_\alpha|^4 \right) \quad , \\ J'_{\mu\nu} &= 2\pi\beta' \cdot T s_{\mu\nu} \quad , \end{aligned} \quad (83)$$

where $s_{\mu\nu}$ was defined in Eq. (59). This is the expected continuum limit of the lattice action $W_{\text{mix}}[V, \phi]$ (cf. Eq. (74)) evaluated on the particular saddle-point characterized by β' . Following Refs. [24, 25], we will consider only the k -Antisymmetric representations, as the associated flux tubes are expected to have the lowest action for a given N -ality k :

$$\beta' = \beta^{(k)} = 2N\omega^{(k)} \quad , \quad (84)$$

where $\omega^{(k)}$ is a weight of the k -Antisymmetric representation, say the highest ($\omega^{(k)} = \omega_1 + \dots + \omega_k$). For the lowest action, ξ is the polar angle φ with respect to the x_1 -axis (γ is a straight line). Because of cylindrical symmetry, Eqs. (81) and (82) are solved with

$$\Lambda_\mu = a(\rho, x_1) \partial_\mu \varphi \beta^{(k)} \cdot T \quad , \quad \phi_\alpha = h_\alpha(\rho, x_1) e^{i\beta^{(k)} \cdot \alpha \varphi} \quad , \quad (85)$$

where a, h are real profiles. In order to have a finite action and well-defined regular fields, the appropriate conditions are $a(\rho, x_1) \rightarrow 1$, $h_\alpha(\rho, x_1) \rightarrow v$, when $\rho \rightarrow \infty$. In addition $a(0, x_1)$ and $h(0, x_1)$ must vanish between the quarks and tend to 1 and v , respectively, on the lines belonging to $S(\mathcal{C}_e)$, so as to cancel the effect of $J'_{\mu\nu}$. For asymptotic separations between the quark-antiquark pair, the saddle-point equations are

$$\begin{aligned} \partial_\rho^2 h_\alpha + \frac{\partial_\rho h_\alpha}{\rho} - \frac{(a-1)^2}{\rho^2} (\beta^{(k)} \cdot \alpha)^2 &= m^2 h_\alpha + 2\tilde{\lambda} h_\alpha^3 \quad , \\ \gamma \vartheta^2 \beta^{(k)} \left(\partial_\rho^2 a + \frac{\partial_\rho a}{\rho} \right) &= 2 \sum_\alpha \alpha h_\alpha^2 \beta^{(k)} \cdot \alpha (a-1) \quad . \end{aligned} \quad (86)$$

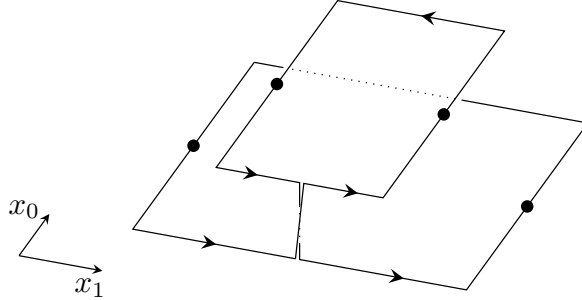


Figure 7: Double-winding Wilson loop: the transverse shift is given by δz .

Regarding the product $\beta^{(k)} \cdot \alpha$ which appears in Eq. (86), there are $k(N - k)$ roots for which it is ± 1 , while the remaining are zero. Hence, it is natural to divide the profiles into two types [26]:

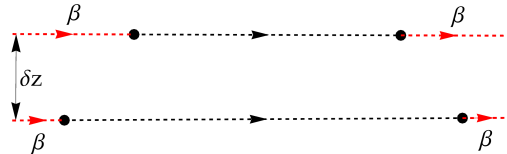
$$\begin{aligned} h_\alpha = h & \quad , \quad \alpha \cdot \beta^{(k)} = 1 \quad , \\ h_\alpha = v & \quad , \quad \alpha \cdot \beta^{(k)} = 0 \quad . \end{aligned} \quad (87)$$

Because of the property $\sum_\alpha \alpha^p \alpha^q = \delta^{pq}/2$, the ansatz closes. Therefore, there is a collective behaviour, where $k(N - k)$ equal profiles satisfy nontrivial equations of motion. Because of the arguments already given in that reference, this leads to Casimir scaling. It is important to underline that the Abelian action $S(J')$ is not physically equivalent to the model defined by $W_{\text{mix}}[V, \phi]$, which only depends on the value of k (modulo N). In our context, $S(J')$ only applies to a particular solution of the lattice model in the continuum. For the collimated fluxes in center-vortex/monopole chains, the Wilson loop only sees linking numbers. In this case, the probability for a center-vortex branch to leave a monopole in a given direction is distributed isotropically. In contrast, in monopole-only scenarios, it is the flux from the monopoles that spreads isotropically, thus giving weight-dependent fluxes through \mathcal{C}_e . In this respect, it is instructive to discuss the double-winding Wilson loop for quarks in the defining representation of $SU(N)$. This observable was proposed in Ref. [53] to differentiate between center-vortex and monopole-only dual superconductor scenarios, as in $SU(2)$ they predict a difference-of-areas and sum-of-areas law, respectively. In that work, the full Monte Carlo lattice simulation of $SU(2)$ Yang-Mills theory ultimately established the validity of the first option.

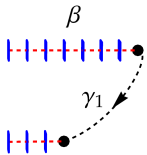
Double-winding Wilson loops

Let us discuss the shifted rectangular double-winding Wilson loop (see Fig. 7) in light of the lattice model for the mixed ensemble of center vortices and chains, comparing it with the monopole-only ensemble in Appendix B. The latter describes compact Cartan gauge fields A_μ and a gas of monopole worldlines carrying all possible adjoint charges α . In this case, the Wilson loop for fundamental quarks can be obtained from its dual version, where a gauge field λ_μ is originated after performing a Hubbard-Stratonovich transformation and solving the constraint imposed by the integration over all possible Cartan gauge fields A_μ . At the end, the monopole-only dual action has the same form of $S(J)$ in Eq. (83), with $J_{\mu\nu} = 2\pi\beta \cdot T s_{\mu\nu}$ and β being any magnetic weight of the defining representation. This type of dual superconductor model was introduced in Ref. [54] and reviewed in [55]. For general $SU(N)$, at a fixed intermediate time, as the charge β is carried all along the double-winding loop \mathcal{C}_e , the sources depicted in Fig. 8a are obtained. As discussed in Ref. [53], a pair of flux tubes carrying flux β , from left to right, will be induced. When δz is

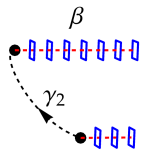
lowered, there could be an interaction between them, which depends on the dual superconductor type. Anyway, the associated law will be approximately given by the sum of areas spanned by the flux tubes. For the mixed ensemble of center vortices and chains, the lattice action is given by



(a) Monopole-only dual superconductor.



(b) Center vortices and chains: $SU(2)$.



(c) Center vortices and chains: $SU(3)$.

Figure 8: Double-winding Wilson loop at an intermediate time-slice $x_0 = 0$, where we see two quarks (antiquarks) on the left (right). We use the same conventions of Fig. 6.

$W_{\text{mix}}[V, \phi]$ in Eq. (74), with $b(p) = (2\pi/N) s(p)$ and $s(p)$ nontrivial only when p intersects a surface whose border is \mathcal{C}_e . Again, when it comes to determining the lowest action, we must determine the best weight distribution for a fixed frustration $e^{ib(p)}$. When δz is small, as the continuum is approached, the lowest action will be characterized by a pair of angles ξ_1, ξ_2 , multivalued with respect to paths γ_1, γ_2 . They are shown for $SU(2)$ and $SU(3)$ in Figs. 8b and 8c, respectively. In each case, away from the quarks, the fields will be given by Eq. (76), with

$$\Delta(l) = \begin{cases} \beta \Delta_l \xi_1 + \beta \Delta_l \xi_2, & \beta = \sqrt{2} \\ \beta_1 \Delta_l \xi_1 + \beta_2 \Delta_l \xi_2, & \beta_1 = (\sqrt{3}, 1), \quad \beta_2 = (-\sqrt{3}, 1). \end{cases} \quad (88)$$

Indeed, these configurations give the same frustration in the upper and lower plaquettes, as required: for $SU(2)$, $e^{i\pm 2\pi\beta \cdot T} = e^{\pm i\pi\sigma_3} = -I$, while for $SU(3)$, $e^{i2\pi\beta_1 \cdot T} = e^{i2\pi\beta_2 \cdot T} = e^{-i\frac{2\pi}{3}} I$. In the first case, the action will be concentrated on a pair of flux tubes on top of the curves γ_1, γ_2 formed by the red and black lines in Fig. 8b, thus leading to a difference-of-areas law. In the second case, as $\beta_1 + \beta_2 = -\beta_3$, it is clear that, in the global minimization, it is energetically favorable for the flux tubes to coalesce into a single one, leading to the double-Y shaped flux tube depicted in Fig. 8c. In this case, the paths γ_1 and γ_2 join at the left junction and continue up to the right junction where they separate.

E. The effect of monopole matching

It is easy to see that the matching of three monopole worldlines at a point is generated by adding the following cubic term in the potential $\mathcal{U}(\phi)$ of Eq. (74):

$$ac_{\alpha\gamma\delta} \phi_\alpha \phi_\gamma \phi_\delta, \quad (89)$$

where we adopted a summation over repeated indices that considers not only positive but also negative roots, with the condition $\phi_{-\alpha} = \bar{\phi}_\alpha$. The coefficients $c_{\alpha\gamma\delta}$ must vanish if the constraint in Eq. (6) is not satisfied. They must also be invariant under root transformations induced by permutations of the defining weights ω_j .⁴ New quartic monopole interactions that contain $|\phi_\alpha|^2|\phi_\beta|^2$ may also be included. Note that the ansatz in Eq. (85) continues to close the flux tube field equations

$$D^2\phi_\alpha = m^2\phi_\alpha + 2\tilde{\lambda}\phi_\alpha(\bar{\phi}_\alpha\phi_\alpha) + 3c_{-\alpha\gamma\delta}\phi_\gamma\phi_\delta + \dots ,$$

as the monopole-matching constraint yields

$$\phi_\gamma\phi_\delta = h_\gamma h_\delta e^{i\beta\cdot\gamma\varphi} e^{i\beta\cdot\delta\varphi} = h_\gamma h_\delta e^{i\beta\cdot\alpha\varphi} .$$

As a consequence, even in the Abelian-projected setting, the field profiles are not necessarily of the Nielsen-Olesen type and the asymptotic Casimir scaling could only be approximately satisfied.

VII. ENSEMBLES WITH LOCAL D.O.F.

In the previous section, the Abelian projected scenario was translated from the continuum Hamiltonian formalism to the lattice 4D partition function. The N types of worldsurfaces with global charges were generated by a complex diagonal $N \times N$ matrix $V(x, y)$. Here, using the Weingarten representation of surfaces and loops, we revisit the 4D mixed ensemble with non-Abelian d.o.f. of Ref. [18] (cf. Eq. (12)). Here, our main focus will be oriented to compare this possibility with the Abelian projected scenario. Let us initially consider center-vortex worldsurfaces generated by general link-variables $V(x, y) \in \mathbb{C}^{N \times N}$ governed by the lattice action (68). As already discussed in Sec. III, the quartic model generates surfaces with N possible ‘‘colors’’ at each vertex, stabilized by contact interactions. In the γ expansion, if a given link is only occupied by N variables $V(x, y)$, the contribution is zero. The situation changes when this is combined with a factor originating from the expansion of a new term in the action $\xi(\det V(x, y) + \det V(y, x))$. Because of this N -matching property, the symmetry is reduced to

$$V(x, y) \rightarrow U(x)V(x, y)U^{-1}(y) \quad , \quad U \in SU(N) . \quad (90)$$

To generate chains, we can proceed as in Sec. VIB, but taking into account the non-Abelian properties of $V(x, y)$. The monopole loops are again introduced according to the discussion in Sec. V. They are generated by monopole fields ζ_α in the adjoint representation of $SU(N)$

$$\begin{aligned} Z_{\text{mix}}[b] &\propto \int DV D\zeta \exp(-W_{\text{mix}}[V, \zeta]) \quad , \quad W_{\text{mix}}[V, \zeta] = W_{\text{c.v.}}[V] - \sum_l \tilde{V}(l) + \tilde{Q}[\zeta] \\ \tilde{V}(l) &= \sum_\alpha \zeta_\alpha^\dagger(x) H(x, y) \zeta_\alpha(y) \quad , \quad H(x, y)|_{AB} = \text{Tr}(V(x, y)T_B V^\dagger(x, y)T_A) , \\ \tilde{Q}[\zeta] &= \sum_x \sum_\alpha \tilde{Q}(\zeta_\alpha(x)) \quad , \quad \tilde{Q}(\zeta) = \tilde{\eta} \zeta^\dagger \zeta + \tilde{\lambda} (\zeta^\dagger \zeta)^2 . \end{aligned} \quad (91)$$

The interpolation property between pairs of center-vortex worldsurfaces can be analyzed as already done for the Abelian projected case. This time, expanding in $\tilde{V}(l)$ and integrating over V , there are contributions that involve the loop variables

$$\text{Tr} H(x_1, x_2) \dots H(x_n, x_1) . \quad (92)$$

⁴ The different roots α_{ij} are given by the $N(N-1)$ possible values of $\omega_i - \omega_j$.

In addition, Eq. (90) implies

$$H(x, y) \rightarrow R(x)H(x, y)R^{-1}(y) \quad , \quad UT_AU^{-1} = T_BR(U)|_{BA} \quad , \quad (93)$$

so that the model still has the local symmetry (90), as long as

$$\zeta_\alpha(x) \rightarrow R(x)\zeta_\alpha(x) \quad (94)$$

($R = R(U)$ is the adjoint representation of U). Therefore, the ensemble $Z_{\text{mix}}[b]$ also contains center-vortex worldsheets attached to monopole worldlines, which are associated to $SU(N)$ -singlets in the γ expansion. Now, we can follow the same series of steps as in the Abelian projected case. As discussed in the general Weingarten framework, when (center-vortex) worldsheets percolate, $V(x, y)$ is forced to be close to $\vartheta U(x, y)$, $U(x, y) \in U(N)$. In addition, we shall assume the effect of N -matching to be strong (large ξ), which drives $U(x, y)$ close to $SU(N)$. Then, when this initial stage dominates, the monopole sector can be approximated by Eq. (56) with $\tilde{\gamma} = \vartheta^2$ and $R(x, y) = R(U(x, y))$, $U(x, y) \in SU(N)$. That is, the model becomes

$$W_{\text{mix}}[V, \zeta] \approx \gamma \vartheta^2 \sum_p \text{Tr} \left(I - e^{ib(p)} U(p) \right) + \vartheta^2 \sum_{x, \mu} \sum_\alpha (\Delta_\mu \zeta_\alpha)^\dagger \Delta_\mu \zeta_\alpha + \mathcal{U}(\zeta) \quad , \quad (95)$$

$$\Delta_\mu \zeta = R(x, x + \mu) \zeta(x + \mu) - \zeta(x) \quad , \quad \mathcal{U}(\zeta) = \sum_x \sum_\alpha \left(a^2 m^2 |\zeta_\alpha|^2 + \tilde{\lambda} |\zeta_\alpha|^4 \right) \quad . \quad (96)$$

A. Non-Abelian scenario and the confining flux tube

The different adjoint flavors ζ_α in Eq. (96) are uncorrelated, so that $N(N - 1)$ independent ensembles of loops $\text{Tr} \Gamma_R(\mathcal{C})$ labeled by the adjoint weights α are generated (see Eq. (54)). Up to this point, there is only repulsion between worldlines of the same type α . However, this could compete with other interactions and natural correlations, such as the monopole matching properties considered in Ref. [18] (see Sec. II 4). Cubic and quartic interactions were exhaustively reviewed and analyzed in Ref. [26]. In fact, in the non-Abelian case, they are essential to drive a phase that supports the formation of a confining flux tube. Otherwise, the vacua manifold would be the product of $N(N - 1)/2$ higher dimensional spheres $\bar{\zeta}_\alpha^A \zeta_\alpha^A = v^2$ (no summation over α). In the continuum limit this would imply a trivial first homotopy group. In the non-Abelian lattice scenario, three-line matching may be included by the cubic term:

$$a\kappa N_{\alpha\gamma} (\zeta_{\alpha+\gamma}^\dagger, [\zeta_\alpha, \zeta_\gamma]) = a\kappa N_{\alpha\gamma\delta} (\zeta_\delta, [\zeta_\alpha, \zeta_\gamma]) \quad , \quad \zeta_{-\alpha} = \zeta_\alpha^\dagger \quad . \quad (97)$$

Here, instead of a column matrix with components ζ^A , we changed the notation to use Lie algebra valued fields $\zeta = \zeta^A T_A$. The structure constants follow the conventions of Ref. [26]. As usual, $N_{\alpha\gamma}$ is only nonzero when $\alpha + \gamma$ is a root. This root can always be written as $-\delta$, where δ is a root. This defines the structure constants in the second member that only contribute when $\alpha + \gamma + \delta = 0$. In this notation, the covariant derivative and the transformation of monopole fields read

$$\Delta_\mu \zeta = U(x, x + \mu) \zeta(x + \mu) U(x + \mu, x) - \zeta(x) \quad , \quad \zeta(x) \rightarrow U(x) \zeta(x) U^{-1}(x) \quad . \quad (98)$$

The important point is that the additional interactions can easily generate a monopole condensate such that the system undergoes $SU(N) \rightarrow Z(N)$ SSB [26], which gives a vacua manifold with nontrivial first homotopy group

$$\Pi_1(SU(N)/Z(N)) = Z(N) \quad . \quad (99)$$

In the continuum limit, this will lead to topological solutions with N -ality properties, such as confining flux tubes with center-charges (k -strings) [56–61]. In the lattice, similarly to the Abelian projected case, the following conditions must be approximately satisfied away from the quarks:

$$U(p) = e^{-ib(p)} I \quad , \quad U(x, y)\zeta_\alpha(y)U(y, x) = \zeta_\alpha(x) . \quad (100)$$

In addition, the monopole fields must be close to the vacua manifold, which can be assumed to be $\zeta_\alpha = vUE_\alpha U^{-1}$. Although this is not the most general form, it occurs in a large class of $SU(N) \rightarrow Z(N)$ SSB models. By the same arguments presented in the Abelian case, we must have

$$U(x, y) = U(x) e^{i\Delta(l)\cdot T} U^{-1}(y) \quad , \quad \Delta(l) = \beta' \Delta_l \xi , \quad (101)$$

where $\Delta_l \xi$ was defined after Eq. (79) and $U(x) \in SU(N)$ is an arbitrary field defined at the sites. That is, a general weight β' with N -ality k comes into play, not necessarily equal to β_e , to be determined by lowering the associated saddle-point action. Again, the monopole fields are consistently defined at the sites as starting from $\zeta_\alpha(x)$, applying Eq. (100) to consecutive links along a closed path, we return to $\zeta_\alpha(x)$. When $k = 0$, there is no frustration and no confining string. For nontrivial k , with $U_\mu(x, y) = e^{ia\Lambda_\mu(x)}$, $\Lambda_\mu \in \mathfrak{su}(N)$, the continuum version of the saddle-point equations can be used to determine which β' leads to the lowest action

$$S(J') = \int d^4x \left(\frac{\gamma\vartheta^2}{4} (F_{\mu\nu} - J'_{\mu\nu})^2 + \frac{1}{2} \left((D_\mu \zeta_\alpha)^\dagger, D_\mu \zeta_\alpha \right) + \mathcal{U}(\zeta) \right) , \quad (102)$$

where $J'_{\mu\nu}$ was defined in Eq. (83). These equations were extensively analyzed in Ref. [26], with the lowest action given by the antisymmetric weight $\beta^{(k)}$. Similarly to the Abelian projected case, as the parameters are changed, these models allow for different flux tube profiles that could fit the lattice data produced at asymptotic distances.

B. Comparing Abelian projected and non-Abelian scenarios

To better compare the scenarios, note that the Abelian projected model (70) is embedded in the non-Abelian one by simply considering $V(x, y)$ diagonal and $\zeta_\alpha = \phi_\alpha E_\alpha$. In this case⁵

$$\tilde{V}(l) = \sum_\alpha \bar{\phi}_\alpha(x) \phi_\alpha(y) \text{Tr}(V(x, y) E_\alpha V^\dagger(x, y) E_\alpha^\dagger) = \frac{1}{2N} \sum_{i < j} \bar{\phi}_{ij}(x) \phi_{ij}(y) \bar{V}_j(x, y) V_i(x, y) . \quad (103)$$

In particular, when center vortices condense, Eq. (74) can be encoded in Eqs. (95), (96) with

$$U(x, y) = \begin{pmatrix} U_1 & 0 & \cdots & 0 \\ 0 & U_2 & \cdots & 0 \\ \vdots & \vdots & \ddots & \vdots \\ 0 & 0 & \cdots & U_N \end{pmatrix} , \quad \prod_i U_i = 1 \quad , \quad \zeta_\alpha = \phi_\alpha E_\alpha \quad (104)$$

(no summation over α). Also, the cubic term (89) is embedded in the form (97), with $c_{\alpha\gamma\delta} = \kappa N_{\alpha\gamma\delta}^2$. When $c_{\alpha\gamma\delta}$ is negative, the fusion of three monopole charges is favored. This corresponds to $\kappa < 0$, which is also required to drive the above mentioned $SU(N) \rightarrow Z(N)$ SSB pattern. Now, let us consider the mixed ensemble partition function (95), with $\mathcal{U}(\zeta)$ containing the additional interactions required to drive this pattern. Of course, all possible configurations, Abelian-like or

⁵ The only nontrivial element of the matrix E_α , $\alpha_{ij} = \omega_i - \omega_j$, is at the ij position.

not, will be present. However, when computing the Wilson loop, the relevant ones are expected to be distributed around a flux tube characterized by the antisymmetric weight with the same N -ality of the quarks representation $D(\cdot)$. Indeed, as shown in Ref. [26], there is a region in parameter space where the solutions have the Abelianized form $\zeta_\alpha = \phi_\alpha E_\alpha$, together with Eq. (85). This is a stable region in the sense that, under small deviations, the action continues to be bounded from below and the associated properties are only perturbatively modified. That is, for the Wilson loop calculation, the relevant center-vortex worldsheets with N local ‘‘colors’’ at the vertices essentially behave as N surface types with global charges β_i . For this reason, in the lattice, the Abelian projected and non-Abelian models are expected to share various properties at asymptotically large distances between quark probes.

1. Common features

- N -ality: This includes, the difference-of-areas law for double Wilson loops (in $SU(2)$) [53] and double Y-shaped potentials [62] (see Sec. VID).
- Regarding the flux tube, the following properties are expected to be accommodated at the same time:
 - Asymptotic Casimir law $\propto k(N-k)$. Present lattice data place the string tension somewhere between this behavior and the sine law [63].
 - k -independent transverse profiles.
 - Nielsen-Olesen transverse distribution. Lattice studies done in Refs. [64], [65] mainly explored intermediate distances. At asymptotically large distances, the data still present large error bars.

These properties would occur at specific regions in parameter space. In both models, departures can be easily parametrized and could be adjusted to lattice data.

- The three-line monopole matching can change the phase transition to be first order. This type of matching only exists for $N \geq 3$. For $N = 2$ there are just two (one-component) roots $\alpha = \pm 1/\sqrt{2}$. It is satisfying to note that the confinement/deconfinement phase transition is known to be first (second) order for $N \geq 3$ ($N = 2$).

2. Differences

In the continuum, unlike the Abelian projected case, where $S(J')$ in Eq. (83) is only used to evaluate the action of a particular solution, in the non-Abelian case it can also be used for the global minimization problem. This is because of the topological properties implied by Eq. (99). Even if β' is not an antisymmetric weight $\beta^{(k)}$, the global minimization will be able to transition to $\beta^{(k)}$. For example, for adjoint quarks, if we start with $\beta_e = 2N\alpha$, the minimization gives a vanishing action. This is attained for a well-defined non-Abelian single-valued solution

$$\Lambda_\mu = iS\partial_\mu S^{-1} \quad , \quad \zeta_\alpha = vSE_\alpha S^{-1} \quad , \quad (105)$$

which cancels the effect of the sources (see Ref. [66]). Therefore, in the non-Abelian case, the continuum limit of $Z_{\text{mix}}[b]$ is expected to be captured by the partition function:

$$Z_{\text{mix}}[J_e] = \int [\mathcal{D}\Lambda_\mu][\mathcal{D}\zeta] e^{-S(J_e)} \quad , \quad J_e|_{\mu\nu} = 2\pi\beta_e \cdot Ts_{\mu\nu} \quad . \quad (106)$$

Another difference relates to the possibility of extending the model to the intermediate confining region, where the flux tube tension scales with the quadratic Casimir of the quark representation [67]. In this regime, the total energy stored in the adjoint string is smaller than the energy required to screen the adjoint quark probes [68]. It is well-known that Abelian projection cannot describe this regime. For a general ensemble formed by thick configurations, when considering the adjoint representation, not all the terms in Eq. (58) give the same average. In this case, there are always vanishing weights, so that the average $\langle \mathcal{W}_{\text{Ad}}(\mathcal{C}_e) \rangle$ is never exponentially suppressed. On the other hand, the combined effect of center-vortex stiffness and domains characterized by general non-Abelian orientations was advocated as a possible explanation for the intermediate Casimir scaling [42, 43]. Then, in the non-Abelian ensemble, there is still the possibility to include the effect of center-vortex thickness to get a smoother transition from the asymptotic to the intermediate region. An investigation in this direction will be presented elsewhere.

VIII. CONCLUSIONS

In this work, relying on the Weingarten matrix representation of surfaces, we compared the Abelian-projected and the non-Abelian mixed ensembles of percolating center vortices and chains. Initially, we noted that the model based on $V(x, y) \in \mathbb{C}^{N \times N}$ matrix link-variables with Gaussian weight describes the ensemble of closed noninteracting surfaces with N possible colors at their vertices. In the Abelian projected case, the elementary center-vortex worldsheets are characterized by global magnetic weights β_i of the defining representation, which are physically equivalent. Then, the ensemble was generated by N variables $V_i(x, y) \in \mathbb{C}$ with a symmetry under permutations of the labels. In the non-Abelian case, the center-vortex worldsheets were generated by a single matrix-valued variable $V(x, y) \in \mathbb{C}^{N \times N}$. Here, the N possible colors at each vertex correspond to a magnetic charge β_i that can change from point to point over the surface.

The noninteracting $V(x, y) \in \mathbb{C}^{N \times N}$ model served as a basis to include the properties that turn the surfaces into center-vortex worldsheets and chains. As is well-known, this model is in fact unstable. Then, the next step was to introduce an appropriate stabilizing quartic term that provides contact interactions. This way, not only the normal but also the percolating phase was stabilized. Here, the interesting result is that, as the effect of the quartic term gets stronger, the percolating phase becomes described by gauge field link-variables governed by the Wilson action with $U(N)$ local symmetry. That is, we extended the result of Ref. [22] to the non-Abelian case. In this reference, the Goldstone modes of a condensate of Abelian loops, which span oriented closed surfaces, were shown to be described by a $U(1)$ gauge field. Returning to the center-vortex context, one of the defining properties of worldsheets is that they generate a center element when the Wilson loop is linked. Another fingerprint is the natural matching between N different center-vortex fluxes β_i , as the total flux is conserved due to the property $\beta_1 + \dots + \beta_N = 0$ (N -matching). They were introduced by means of an appropriate lattice frustration and a new term in the Weingarten model. In the Abelian-projected setting, this term has the form $\propto V_1(x, y) \dots V_N(x, y)$, which reduces the local symmetry from $U(1)^N$ to $U(1)^{N-1}$. Similarly to Ref. [18], center-vortex worldsheets with different weights β_i, β_j attached in pairs to monopole worldlines (chains) were simply introduced by means of additional scalar fields. When N -matching is strongly favored, the percolating phase can be approximated by the Wilson action for $U(1)^{N-1}$ gauge fields minimally coupled to the monopole scalars. That is, elementary center vortices and chains provide emergent gauge fields, monopole scalars, and minimal coupling. In the continuum, these are fundamental properties to generate a topologically stable flux tube. Up to this point, this ensemble describes the same physics already parametrized in the wavefunctional approach. Then, it comes as no surprise that, as the continuum limit is approached, percolating center vortices and monopoles lead to a minimal area law

with N -ality and asymptotic Casimir scaling. This line of thought parallels that proposed in Ref. [18], which was revisited here by analyzing the $V(x, y) \in \mathbb{C}^{N \times N}$ model. In this case, N -matching changes the local symmetry from $U(N)$ to $SU(N)$. In the phase where percolation and N -matching dominate, the variables become approximated by $SU(N)$ lattice gauge fields, while chains are generated by minimally coupled adjoint monopole fields. This time, as already discussed in detail in previous works, additional natural correlations are essential to generate a flux tube. Among them, the matching of three worldlines carrying adjoint weights such that $\alpha + \gamma + \delta = 0$ and additional quartic interactions can drive $SU(N) \rightarrow Z(N)$ SSB. In Ref. [26], the different possibilities were analyzed in the continuum. In particular, there are conditions on the parameters such that the Nielsen-Olesen profiles and the asymptotic Casimir law is exact. That is, although we initially considered worldsheets with magnetic weights changing from point to point, the series of phase transitions favors worldsheets with global weights. On the other hand, these models have a rich parameter space with a variety of asymptotic properties that could fit the flux tube lattice data and the order of the phase transition. In fact, this is also true in the Abelian-projected setting, when the matching of three monopole worldlines and other interactions are included. Regarding the lines that could be pursued, as the proposed modeling is able to interpolate the percolating and normal phases, it would be interesting to analyze whether it can capture the geometry of center-vortex worldsheets observed at finite temperature in Ref. [69]. Also, essentially non-Abelian behavior, such as the screening by valence gluons and intermediate Casimir scaling, could be captured by appropriate physically motivated extensions of the proposed lattice models.

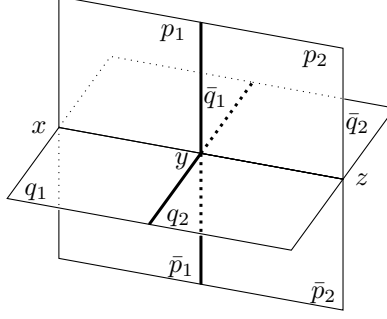


Figure 9: Two consecutive arrays of four plaquettes (oriented as in Fig. 3a).

Appendix A: Surfaces in contact

For the array of four plaquettes depicted in Fig. 3a, using the Gaussian integral

$$\begin{aligned} & \int dV \operatorname{Tr}(VA) \operatorname{Tr}(V^\dagger B) \operatorname{Tr}(VC) \operatorname{Tr}(V^\dagger D) e^{-\mathcal{Q}_0(V)} \\ &= \operatorname{Tr}(AB) \operatorname{Tr}(CD) + \operatorname{Tr}(AD) \operatorname{Tr}(CB) , \end{aligned} \quad (\text{A1})$$

we get the partial contribution

$$\begin{aligned} C(p, \bar{p}, q, \bar{q}) &= \int dV(x, y) \operatorname{Tr}V(p) \operatorname{Tr}V(\bar{p}) \operatorname{Tr}V(q) \operatorname{Tr}V(\bar{q}) e^{-\mathcal{Q}_0(V(x, y))} \\ &= \operatorname{Tr}(\Gamma(\partial(p \cup \bar{p}))) \operatorname{Tr}(\Gamma(\partial(q \cup \bar{q}))) + \operatorname{Tr}(\Gamma(\partial(p \cup \bar{q}))) \operatorname{Tr}(\Gamma(\partial(q \cup \bar{p}))) . \end{aligned} \quad (\text{A2})$$

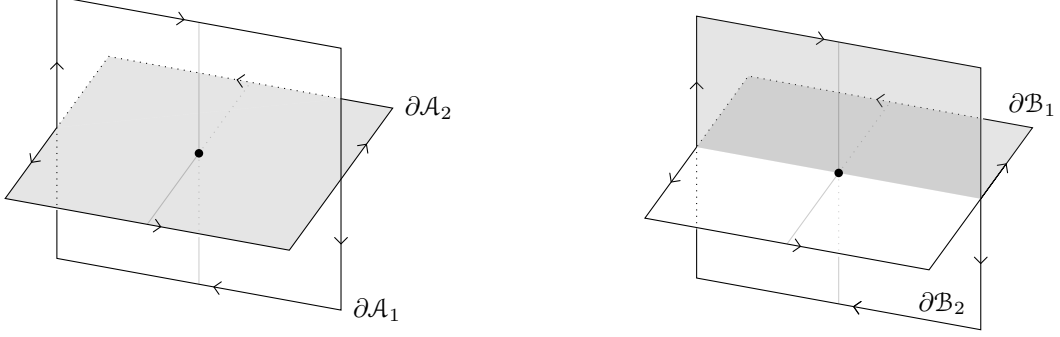
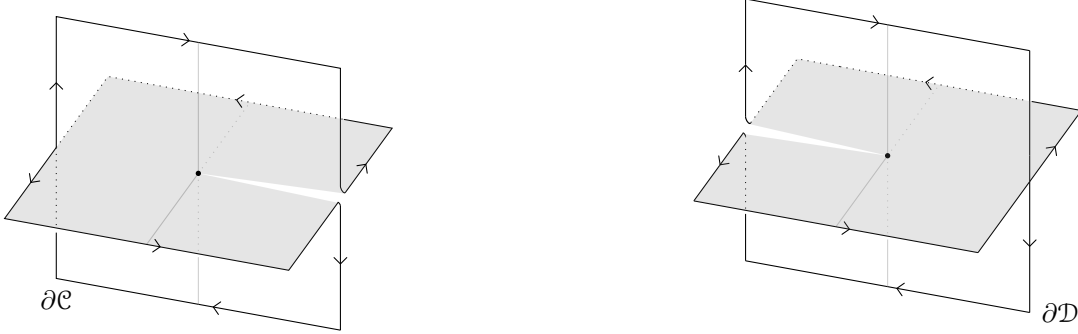
The surface elements associated with the first term (Fig. 3b) have two edges placed at the same link (x, y) , where $p \cup \bar{p}$ intersects $q \cup \bar{q}$. Those associated with the second term (Fig. 3c) have two edges at (x, y) , where $p \cup \bar{q}$ touches $q \cup \bar{p}$. Now, let us consider two consecutive arrays of four plaquettes (see Fig. 9). In the partial contribution, besides the integrals at the doubly occupied links (x, y) , (y, z) on \mathcal{C} , we also perform the integrals over the matrix variables V_i at the four single links where these arrays meet (shown in bold). This implements the “gluings” $p_1 \cup p_2$, $\bar{p}_1 \cup \bar{p}_2$, $q_1 \cup q_2$, $\bar{q}_1 \cup \bar{q}_2$ and yields

$$\begin{aligned} & \int \prod_{i=1}^4 dV_i C(p_1, \bar{p}_1, q_1, \bar{q}_1) C(p_2, \bar{p}_2, q_2, \bar{q}_2) \\ &= N^2 \operatorname{Tr}(\Gamma(\partial \mathcal{A}_1)) \operatorname{Tr}(\Gamma(\partial \mathcal{A}_2)) + N^2 \operatorname{Tr}(\Gamma(\partial \mathcal{B}_1)) \operatorname{Tr}(\Gamma(\partial \mathcal{B}_2)) + N \operatorname{Tr}(\Gamma(\partial \mathcal{C})) + N \operatorname{Tr}(\Gamma(\partial \mathcal{D})) . \end{aligned} \quad (\text{A3})$$

The different paths are shown in Figs. 10 and 11, while the surface elements are given by

$$\begin{aligned} \mathcal{A}_1 &= p_1 \cup \bar{p}_1 \cup \bar{p}_2 \cup p_2 \quad , \quad \mathcal{A}_2 = q_1 \cup \bar{q}_1 \cup \bar{q}_2 \cup q_2 \\ \mathcal{B}_1 &= p_1 \cup \bar{q}_1 \cup \bar{q}_2 \cup p_2 \quad , \quad \mathcal{B}_2 = q_1 \cup \bar{p}_1 \cup \bar{p}_2 \cup q_2 \\ \mathcal{C} &= p_1 \cup \bar{p}_1 \cup \bar{p}_2 \cup q_2 \cup q_1 \cup \bar{q}_1 \cup \bar{q}_2 \cup p_2 \\ \mathcal{D} &= p_1 \cup \bar{q}_1 \cup \bar{q}_2 \cup q_2 \cup q_1 \cup \bar{p}_1 \cup \bar{p}_2 \cup p_2 . \end{aligned} \quad (\text{A4})$$

Here, the ordering specifies how the plaquettes are glued, which defines different orientations (in these sequences, the last plaquette is also glued to the first). Note that at the lattice site y common to the eight plaquettes, \mathcal{A}_1 and \mathcal{A}_2 (\mathcal{B}_1 and \mathcal{B}_2) provide a couple of independent vertices that happen to be at the same place. On the other hand, \mathcal{C} (or \mathcal{D}) is a connected single surface

Figure 10: The paths $\partial A_1, \partial A_2, \partial B_1, \partial B_2$.Figure 11: The paths $\partial C, \partial D$.

element with just one vertex at y . Accordingly, in the first case, the contribution in Eq. (A3) is given by the product of two independent factors like in Eq. (27), while in the second case it is given by just one factor of this type. That is, the factors at y are N^2 or N , depending on whether the number of vertices at that site is two or one, respectively. In addition, in all the cases, the number of edges at \mathcal{C} is twice the number of links. For example, the surface element \mathcal{D} has a pair of edges at (x, y) , where $p_1 \cup \bar{q}_1$ touches $q_1 \cup \bar{p}_1$, and a second pair at (y, z) , where $\bar{q}_2 \cup q_2$ intersects $\bar{p}_2 \cup p_2$ (self-intersection). These conclusions can be generalized to the case where \mathcal{C} turns at a right angle or stops growing. In the quartic model, new surface elements are generated, as Eq. (A1) is replaced by

$$\begin{aligned} & \frac{1}{z} \int dV \text{Tr}(VA)\text{Tr}(V^\dagger B)\text{Tr}(VC)\text{Tr}(V^\dagger D) e^{-\mathcal{Q}(V)} \\ & = \beta_a(\text{Tr}(AB)\text{Tr}(CD) + \text{Tr}(AD)\text{Tr}(CB)) + \beta_b(\text{Tr}(ABCD) + \text{Tr}(ADCB)) . \end{aligned} \quad (\text{A5})$$

Appendix B: Double-winding Wilson loop and the monopole-only average

Here, we shall consider the Wilson loop average in a monopole-only Abelian-projected scenario (non-collimated monopole fluxes). The ensemble is formed by closed worldlines with all possible adjoint charge distributions. For example, a single monopole loop carrying charge α (positive roots of $\mathfrak{su}(N)$) is introduced by a source $\mathcal{J}_{\mu\nu}$, whose divergence is localized at the physical monopole current j_μ

$$\partial_\nu \mathcal{J}_{\mu\nu} = -2\pi 2N j_\mu \quad , \quad j_\mu = \alpha \cdot T \int_\gamma ds \frac{dx_\mu}{ds} \delta(x - x(s)) . \quad (\text{B1})$$

The Wilson loop average for fundamental quarks reads

$$\langle \mathcal{W}(\mathcal{C}_e) \rangle = \sum_{\{\gamma\}} \int [DA] \frac{1}{N} \text{Tr} \left(e^{i \int_{\mathcal{C}_e} dx_\mu A_\mu(x)} \right) e^{-\int d^4x \frac{1}{4g^2} (\mathcal{F}_{\mu\nu}(A) - \mathcal{J}_{\mu\nu})^2} e^{-S(\{\gamma\})}, \quad (\text{B2})$$

where A_μ is in the Cartan subalgebra, $\mathcal{F}_{\mu\nu}$ is the dual field-strength, and $S(\{\gamma\})$ is the monopole action for a given distribution $\{\gamma\}$ of loops and adjoint weights. Performing the trace, we have

$$\langle \mathcal{W}(\mathcal{C}_e) \rangle = \frac{1}{N} \sum_i \sum_{\{\gamma\}} \int [DA] e^{i \int d^4x (\mathcal{F}_{\mu\nu}, \omega_i \cdot T s_{\mu\nu})} e^{-\int d^4x \frac{1}{4g^2} (\mathcal{F}_{\mu\nu}(A) - \mathcal{J}_{\mu\nu})^2} e^{-S(\{\gamma\})}, \quad (\text{B3})$$

where ω_i are the weights of the defining representation, which will give the same contribution when averaged over the ensemble. For this reason, we can consider a particular weight ω . The action for A_μ can be linearized with an auxiliary field $\lambda_{\mu\nu}$:

$$\langle \mathcal{W}(\mathcal{C}_e) \rangle = \sum_{\{\gamma\}} \int [DA] [D\lambda] e^{i \int d^4x (\mathcal{F}_{\mu\nu}, \omega \cdot T s_{\mu\nu})} e^{\int d^4x \left(-\frac{g^2}{4} \lambda_{\mu\nu}^2 + i(\lambda_{\mu\nu}, \mathcal{F}_{\mu\nu} - \mathcal{J}_{\mu\nu}) \right)} e^{-S(\{\gamma\})}. \quad (\text{B4})$$

The integration over A_μ leads to the constraint $\epsilon_{\mu\nu\rho\sigma} \partial_\nu (\omega s_{\rho\sigma} + \lambda_{\rho\sigma}) = 0$, which is solved by

$$\lambda_{\mu\nu} = \partial_\mu \lambda_\nu - \partial_\nu \lambda_\mu - \omega s_{\mu\nu}. \quad (\text{B5})$$

Then, after the field redefinition $2\pi 2N \lambda_\mu \rightarrow \lambda_\mu$, we get

$$\langle \mathcal{W}(\mathcal{C}_e) \rangle = \int [D\lambda] e^{-\int d^4x \frac{1}{\tilde{g}^2} (\partial_\mu \lambda_\nu - \partial_\nu \lambda_\mu - J_{\mu\nu})^2} \sum_{\{\gamma\}} e^{i \int d^4x (\lambda_\mu, j_\mu(\{\gamma\}))} e^{-S(\{\gamma\})}, \quad (\text{B6})$$

where $\beta = 2N\omega$, $J_{\mu\nu} = 2\pi\beta \cdot T s_{\mu\nu}$, and we defined

$$\frac{1}{\tilde{g}^2} = \frac{g^2}{4} \frac{1}{16\pi^2 N^2}. \quad (\text{B7})$$

The monopole currents can be modeled as we did for the collimated case, by assuming independent diluted gases labeled by α . In the continuum, besides a tension parameter, stiffness is required to get a well-defined ensemble. The techniques of Refs. [18, 70–73] can be used to obtain the effective representation

$$\langle \mathcal{W}(\mathcal{C}_e) \rangle = \int [D\lambda] [D\phi_\alpha] e^{-\int d^4x \frac{1}{\tilde{g}^2} (\partial_\mu \lambda_\nu - \partial_\nu \lambda_\mu - J_{\mu\nu})^2} e^{-\sum_\alpha \int d^4x (D_\mu \bar{\phi}_\alpha D_\mu \phi_\alpha + \mathcal{U}(\phi))}, \quad (\text{B8})$$

where ϕ_α are the monopole fields. The action in this representation has the same form as that for the collimated case in Eq. (83). The important difference is that, for a double-winding Wilson loop \mathcal{C}_e there is a single fundamental weight β associated to the whole surface $S(\mathcal{C}_e)$.

ACKNOWLEDGMENTS

We would like to acknowledge D. Weingarten for useful discussions. This work was partially supported by the Conselho Nacional de Desenvolvimento Científico e Tecnológico (CNPq), and the São Paulo Research Foundation (FAPESP), grant no. 2023/18483-0.

[1] S. Kratochvila, P. de Forcrand, Nucl. Phys. B 671 (2003) 103.

- [2] L.D. Debbio, M. Faber, J. Giedt, J. Greensite, S. Olejnik, Phys. Rev. D 55 (1997) 2298.
- [3] L.D. Debbio, M. Faber, J. Giedt, J. Greensite, S. Olejnik, Phys. Rev. D 58 (1998) 094501.
- [4] K. Langfeld, H. Reinhardt, O. Tennert, Phys. Lett. B 419 (1998) 317.
- [5] P. de Forcrand, M. D'Elia, Phys. Rev. Lett. 82 (1999) 4582.
- [6] M.Engelhardt, K.Langfeld, H.Reinhardt, O.Tennert, Phys. Rev. D 61 (2000) 054504.
- [7] M. Engelhardt, H. Reinhardt, Nucl. Phys. B 567 (2000) 249.
- [8] M. Engelhardt, H. Reinhardt, Nucl. Phys. B 585 (2000) 591.
- [9] C. Alexandrou, P. de Forcrand, M. D'Elia, Nucl. Phys. A 663 (2000) 1031.
- [10] M. Faber, J. Greensite, S. Olejnik, J. High Energy Phys. 1 (2001) 053.
- [11] M. Engelhardt, M. Quandt, H. Reinhardt, Nucl Phys. B 685 (2004) 227.
- [12] R. Höllwieser, T. Schweigler, M. Faber, U.M. Heller, Phys. Rev. D 88 (2013) 114505.
- [13] S.M.H. Nejad, M. Faber, R. Höllwieser, J. High Energy Phys. 10 (2015) 108.
- [14] D. Trewartha, W. Kamleh, D. Leinweber, Phys. Rev. D 92 (2015) 074507.
- [15] S. Deldar, Z. Dehghan, M. Faber, R. Golubich, R. Höllwieser, Universe 7 (2021) 130.
- [16] J. C. Biddle, W. Kamleh, D. B. Leinweber, Phys. Rev. D 106 (2022) 054505.
- [17] J. C. Biddle, W. Kamleh, D. B. Leinweber, Phys. Rev. D 107 (2023) 094507.
- [18] L. E. Oxman, Phys. Rev. D 98 (2018) 036018.
- [19] J. Ambjørn, J. Giedt, J. Greensite, J. High Energy Phys. 02 (2000) 033.
- [20] H. Reinhardt, Nucl. Phys. B 628 (2002) 133.
- [21] Y. Hayashi, Y. Tanizaki, Phys. Rev. Lett 133 (2024) 171902.
- [22] S. J. Rey, Phys. Rev. D 40 (1989) 3396.
- [23] D. R. Junior, L. E. Oxman, G. M. Simões, Universe 7 (2021) 253.
- [24] L. E. Oxman and G. M. Simões, Phys. Rev. D 99 (2019) 016011.
- [25] D. R. Junior, L. E. Oxman, G.M. Simões, Phys. Rev. D 102 (2020) 074005.
- [26] D. R. Junior, L. E. Oxman, G. M. Simões, Phys. Rev. D 108 (2023) 094021.
- [27] D. R. Junior, L. E. Oxman, H. Reinhardt, Phys. Rev. D 106 (2022) 114021.
- [28] L.E. Oxman, H. Reinhardt, Eur. Phys. J. D 78 (2018) 177.
- [29] D. R. Junior, L. E. Oxman, G. M. Simões, JHEP 2020 (2020) 180.
- [30] M. Nguyen, T. Sulejmanpasic, M. Ünsal, Arxiv: 2401.04800.
- [31] D. Weingarten, Phys. Lett. B 90 (1980) 280.
- [32] P. Y. Boyko, M. I. Polikarpov, V. I. Zakharov, Nucl. Phys. Proc. Suppl. 119 (2003) 724.
- [33] V. G. Bornyakov, P. Y. Boyko, M. I. Polikarpov, V. I. Zakharov, Nucl Phys. B 672 (2003) 222.
- [34] J. A. Mickleley, W. Kamleh, D. B. Leinweber, Phys. Rev. D 110 (2024) 034516.
- [35] F. Spengler, M. Quandt, H. Reinhardt, Phys. Rev. D 98 (2018) 094508.
- [36] L. E. Oxman, JHEP 3 (2013) 038.
- [37] T. A. DeGrand and D. Toussaint, Phys. Rev. D 22 (1980) 2478.
- [38] L. E. Oxman, G. C. Santos-Rosa, Phys. Rev. D 92 (2015) 125025.
- [39] D. Fiorentini, D. R. Junior, L. E. Oxman, R. F. Sobreiro, Phys. Rev. D 105 (2022) 125015.
- [40] D. Fiorentini, D. R. Junior, L. E. Oxman, G. M. Simões, R. F. Sobreiro, Phys. Rev. D 103 (2021) 114010.
- [41] M. Faber, J. Greensite, S. Olejnik, J. High Energy Phys. 1 (2001) 053.
- [42] M. Faber, J. Greensite, S. Olejnik, Phys. Rev. D 57 (1998) 2603.
- [43] J. Greensite, K. Langfeld, Š. Olejnik, H. Reinhardt, T. Tok, Phys. Rev. D 75 (2007) 034501.
- [44] G. Bali, Phys. Rev. D 62 (2000) 114503.
- [45] H. Kawai, Prog. Theor. Phys., 65 (1981) 351.
- [46] B. Durhuus, J. Ambjørn, T. Jonsson, Quantum Geometry: A Statistical Field Theory Approach; Cambridge University Press: Cambridge, UK, 1997.
- [47] G. 't Hooft, Nucl. Phys. B 72 (1974) 461; B 75 (1974) 461.
- [48] V. A. Kazakov, Phys. Lett. B 128 (1983) 316; JETP 85 (1983) 1887 (Russian edition).
- [49] K. H. O'Brien, J. B. Zuber, Nuclear Physics B 253 (1985) 621.
- [50] I. K. Kostov, Nuclear Physics B 415 (1994) 29.
- [51] I. Klebanov, L. Susskind, Nucl. Phys. B 31 (1988) 175.
- [52] W. A. Bardeen, R. B. Pearson and E. Rabinovici, Phys. Rev. D 21 (1980) 1037.
- [53] J. Greensite, R. Höllwieser, Phys. Rev. D 91 (2015) 054509.
- [54] Y. Matsubara, S. Maedan, T. Suzuki, Prog. Theor. Phys. 84 (1990) 130.

- [55] G. Ripka, Lect.Notes Phys. 639 (2004) 1.
- [56] A. Hanany, D. Tong, JHEP 307 (2003) 037.
- [57] R. Auzzi, S. Bolognesi, J. Evslin, K. Konishi, A. Yung, Nucl. Phys. B 673 (2003) 187.
- [58] M. Shifman, A. Yung, Phys. Rev. D 70 (2004) 045004.
- [59] A. Hanany, D. Tong, JHEP 404 (2004) 066.
- [60] V. Markov, A. Marshakov, A. Yung, Nucl. Phys. B 709 (2005) 267.
- [61] A. Gorsky, M. Shifman, A. Yung, Phys. Rev. D 71 (2005) 045010.
- [62] C. Alexandrou, G. Koutsou, Phys. Rev. D 71 (2005) 014504.
- [63] A. Athenodorou, M. Teper, JHEP 2021 (2021) 82.
- [64] P.Cea, L. Cosmai, F. Cuteri, A. Papa, Phys. Rev. D 95 (2017) 114511.
- [65] R. Yanagihara, M. Kitazawa, Prog. Theor. Exp. Phys. 9 (2019) 093B02; Erratum in Prog. Theor. Exp. Phys. 7 (2020) 079201.
- [66] L. E. Oxman, EPJ Web of Conferences 137 (2017) 03015.
- [67] G. S. Bali, Phys. Rep. 343 (2001) 1.
- [68] S. Kratochvila, P. de Forcrand, Nucl. Phys. B 671 (2003) 103.
- [69] J. A. Mickle, W. Kamleh, D. B. Leinweber Phys. Rev. D 110 (2024) 034516.
- [70] D.C. Morse, G.H. Fredrickson, Phys. Rev. Lett. 73 (1994) 3235.
- [71] G. H. Fredrickson, *The Equilibrium Theory of Inhomogeneous Polymers*, 1st ed.; Clarendon Press: Oxford, UK, 2006.
- [72] H. Kleinert, *Path Integrals in Quantum Mechanics, Statics, Polymer Physics, and Financial Markets*; World Scientific: Singapore, 2006.
- [73] L. E. Oxman, G. C. Santos-Rosa, B. F. I. Teixeira, Jour. Phys. A 47 (2014) 305401.